IN SITU MEASUREMENTS OF THE APPROACH TO SCALING OF COLLOIDAL CLUSTER SIZE DISTRIBUTIONS DURING AGGREGATION

By

Bernard J. Olivier

B.S., Bates College, 1983

A MASTER'S THESIS

submitted in partial fulfillment of the

requirements for the degree

MASTER OF SCIENCE

Department of Physics

KANSAS STATE UNIVERSITY
Manhattan, Kansas

1987

Approved by:

Major Professor

Table of Contents

Acknowledgements

I gratefully acknowledge the momentous yet gratuitous leadership from my friends Chris Sorensen and Tom Taylor. Thank-you Chris Sorensen, Tom Taylor, Fred Merklin, Everett Ramer and Hongxin Zhang for useful discussions. I gratefully acknowledge my advisory committee Chris Sorensen, Al Compaan and Fred Merklin for their suggestions and support. I express my appreciation to Mark Ross, Joe Prockish and Bill Starr for technical services and advice. I thank Connie Schmidt for typing this thesis. Finally, I acknowledge Chris Sorensen and Roberta Hughes for their selfless proofreading of the manuscript.

This work was supported by NSF Grant No. CBT-8603736.

CHAPTER I

Introduction

Monomers, single particles, found in gaseous and liquid suspensions have a tendency to diffuse and aggregate to form clusters. This irreversible aggregation of monomers into clusters and clusters into larger clusters has, within the last five years, become an important topic in both theoretical and experimental physics. There are two principal reasons for this. The first was the computer simulation by Witten and Sander which modeled cluster formation. The second was the computer simulation by Vicsek and Family which monitored the time evolution of cluster number densities.

The computer simulation by Witten and Sander[1] has stimulated interest in the geometric structure of clusters formed from the random motion of Brownian diffusers. Their simulation modeled the single particle growth of a cluster by randomly introducing a single monomer on the boundary of a two-dimensional lattice then letting it random walk until it contacted a seed monomer at the lattice center. After many successive single particle growth steps a product cluster resulted which was open and diffuse, displaying a self-similarity which could be classified with a fractal dimension[2] (see Fig. 1.1). Since then, TEM micrographs have shown clusters from aggregated sols to have self-similar, fractal structures as well.

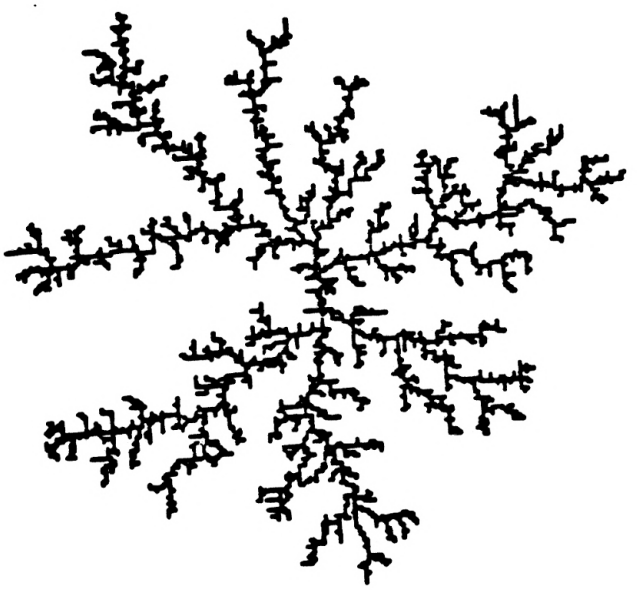

Fig. 1 The Witten and Sanders single particle cluster growth model. A random aggregate of 3600 particles on a square lattice.

If a structure can be divided into sub-sections that are geometrically similar to the encompassing geometry of the whole, the structure is said to be self-similar. The length scale chosen to investigate the self-similarity of a structure is the characteristic length L. The mass of a self-similar structure is related to the characteristic length by

$$M \sim L^{d_f} , \tag{1.1}$$

where d_f is the fractal dimension (see Figure 1.2).

For self-similar particle clusters, the characteristic length is taken as the radius of gyration as measured from the cluster center of mass. The radius of gyration is defined by

$$R_g^2 \equiv \frac{\sum_i r_i^2 m_i}{\sum_i m_i} . \tag{1.2}$$

For us, r_i is the distance from the cluster's center of mass to the i-th monomer of mass m. The static scaling law for the cluster is

$$N \sim R_g^{d_f} , \tag{1.3}$$

where N is the number of monomers making up the cluster. The number of monomers in a cluster is directly proportional to its mass, so expressing the cluster scaling in terms of N is for convenience only. Using the same argument, Eq. (1.3) must hold for the cluster

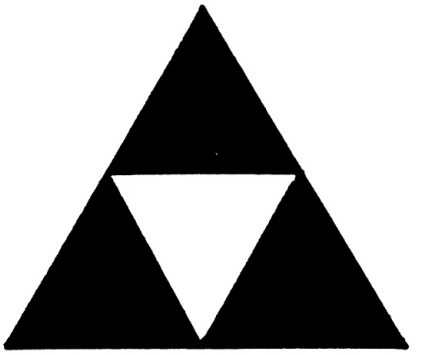

Fig. 1.2a The Sierpinoki Gasket. The self-similarity is evident in the triangular sub-sections. They are similar to the geometry of the whole. This gasket has sides of length 1 and a mass of 3.

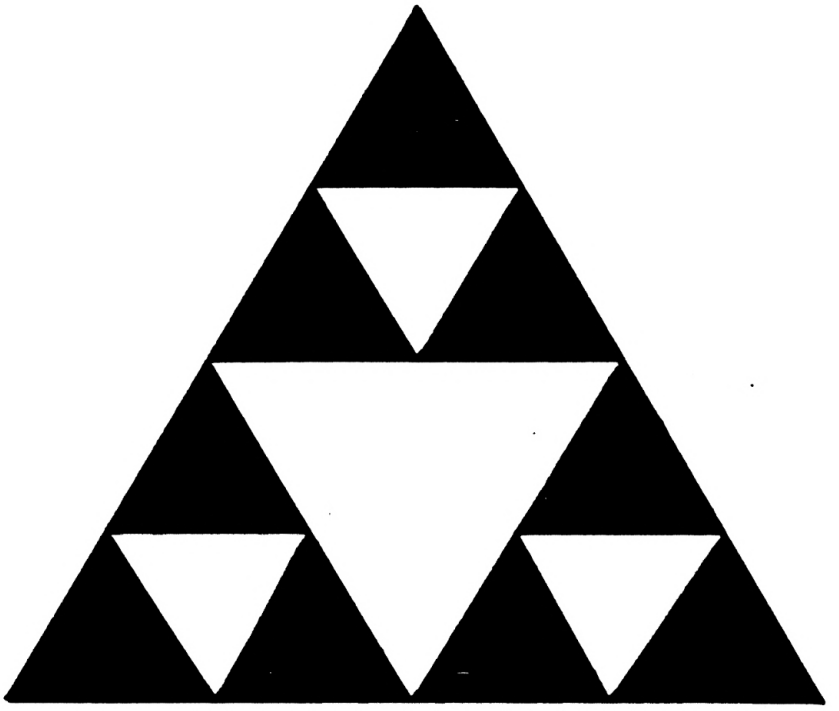

Fig. 1.2b The Scaled Sierpinski Gasket. The sides are of length 2 and the mass is 9. From the static scaling law Eq. (1.2) we find, $d_f = \ln 3/\ln 2$.

volume as well. The fractal dimension of a self-similar cluster is a fraction of the Euclidean space dimension where it exists. This accounts for the diffusiveness of these particle clusters, i.e. as the clusters become infinitely large their densities approach zero. In general, the fractal dimension of a self-similar cluster will depend on the dimension of the space in which it has aggregated and also on its diffusiveness. More diffuse clusters own a smaller fractal dimension.

The dynamic scaling of particle cluster distributions is the second reason for the renewed interest in cluster aggregation. In 1984 Vicsek and Family[3] performed a computer simulation modeling irreversible aggregation and measured cluster number densities as a function of time. Their results indicated that the cluster size distributions obeyed a power law relationship with both the cluster mass and the cluster aggregation time (see Figure 1.3). They found this behavior could be accurately described with the 'scaling' Ansatz

$$n_k(t) \sim t^{-w} k^{-\tau} f(k/t^z) \ . \qquad (1.4)$$

In this expression, $n_k(t)$ is the number of k-mers at time t, k is the number of monomers in a k-mer and t is the aggregation time. The function f(x) is a cutoff function with the asymptotic limits

$$f(x) \sim 1 \quad \text{for } x \ll 1 \qquad (1.5)$$

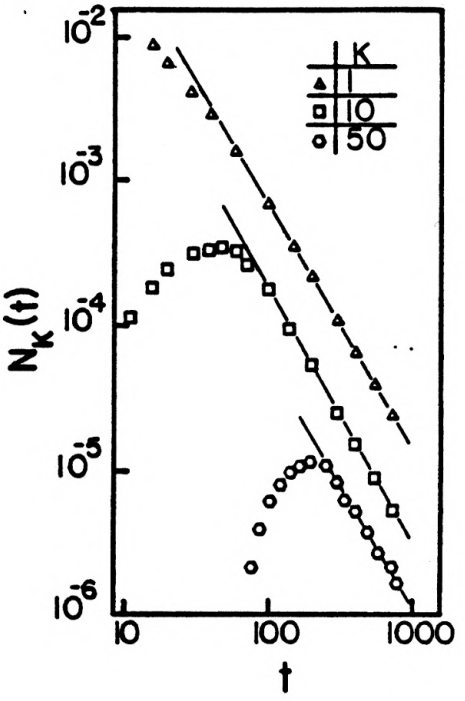

Fig. 1.3a The Viscek and Family cluster aggregation model. This is a log plot of the cluster number density $N_k(t)$ vs. time. The dynamic power law scaling of the Ansatz is indicated by the linear behavior.

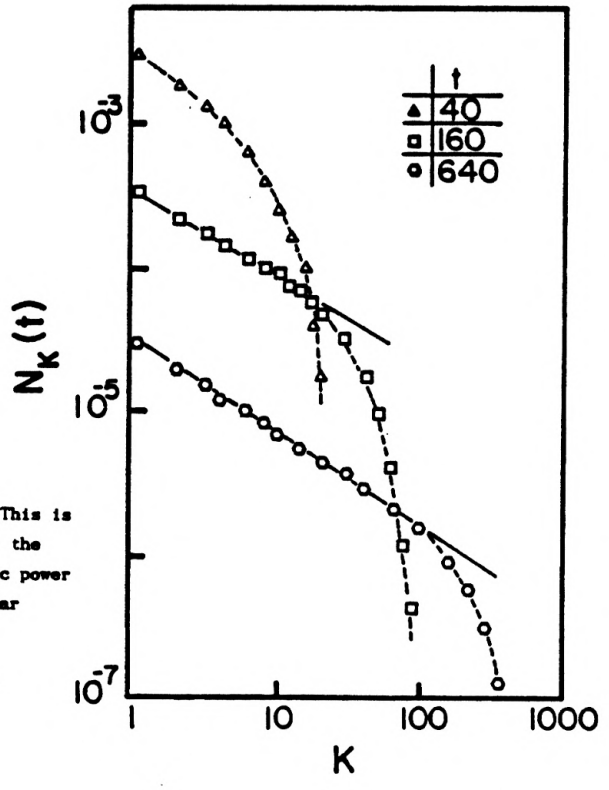

Fig. 1.3b The Viscek and Family cluster aggregation model. This is a log plot of the cluster number density $N_k(t)$ vs. the number of monomers making up a cluster. The static power law scaling of the Ansatz is indicated by the linear behavior.

and

$$f(x) << 1 \quad \text{for } x >> 1 \ , \tag{1.6}$$

where $x = k/t^z$. The expression Eq. (1.4) is valid when the mass of a cluster becomes large and the aggregation time becomes long.

The term 'scaling' Ansatz has been used in reference to Eq. (1.4). The question that needs to be addressed is, "what does it mean for a distribution to be scaling?" If we rewrite Eq. (1.4) as

$$t^w k^\tau n_k(t) \sim f(k/t^z) \ , \tag{1.7}$$

we can arrive at the following general conclusion. Independent of their starting shapes, all distributions when multiplied by the dynamic scaling factor t^w and the static scaling factor k^τ fall on the same universal curve, namely $f(k/t^z)$ when plotted as a function of k/t^z. This can only happen if the shapes of the scaling distributions $n_k(t)$ remain fixed.

Do cluster distributions actually scale? For 'slow' aggregation processes, static measurements have revealed that cluster distributions do scale.[4,5] However, there is no data accounting for the time evolution of a cluster distributing into its final scaling form. How can the evolution of a cluster distribution into its scaling form be described? If a cluster distribution's shape could be monitored while the clusters were aggregating then the scaling behavior could be characterized with an unchanging shape. One could imagine the arbitrary initial shape of a non-scaling distribution evolving into a final unchanging shape, thereby characterizing a scaling distribution.

This thesis focuses on the dynamic scaling behavior of cluster size distributions. In particular, this thesis presents in situ measurements on the dynamic scaling behavior of cluster size distributions.

We will watch the cluster size distributions in gold sols. These colloidal suspensions are initially stable and they are equipped with a relatively narrow distribution of gold monomers. The gold monomers carry an excess of like charge and therefore the suspensions are stabilized by Coulombic repulsions. The suspensions are destabilized by reducing the net charge on each monomer. As a consequence, aggregation is induced and time-dependent cluster distributions result.

All cluster size distributions have a unique set of moments $\{M_N\}$ associated with them. Because of this, it is common to classify cluster distributions in terms of their moments.

Knowing that moments can characterize a distribution, we use the dynamic light-scattering technique, photon correlation spectroscopy, as a probe for investigating the time evolution of the cluster size distributions in aggregating gold sols. Dynamic light-scattering measures the intensity-weighted moments of distributions. In particular, the first two cumulants μ_1 and μ_2 of the dynamic light-scattering spectrum are intensity-weighted moments with a time dependence. We will show the time dependent behavior of μ_1 and μ_2 to be directly related to the evolving shape of a cluster size distribution.

In this thesis, photon correlation spectroscopy was used to measure the time evolution of μ_1 and μ_2 from aggregating gold sols. The two cumulants showed characteristic behaviors for all experimental runs. For example, an effective relative width for a cluster distribution is commonly defined by the ratio $Q \equiv \mu_2/\mu_1^2$. Q has shown the characteristic behavior of approaching nearly the same asymptotic values for all aggregated sols. Also, at the same time during a particular aggregation process that Q appeared to go asymptotic, μ_1 exhibited a dynamic scaling that was power law in time. The approach of Q to an asymptotic constant and the dynamic scaling of μ_1 happened within a few characteristic times from the onset of aggregation in all the sols. These results are explained by considering the general behavior of the asymptotic moments from the scaling Ansatz, the aggregation kinetics describing the dynamics between the aggregating clusters, and the fractal nature of the clusters.

CHAPTER II

Theory

A. Moments of the Scaling Ansatz

Although the exponents w, τ, and z cannot be explicitly determined without considering the kinetics involved during aggregation, we can get a feeling for their physical representation by considering the first two moments of the asymptotic distribution [see Eq. (1.4)].

The first moment of any distribution is defined by

$$M_1 = \sum_{k=1}^{\infty} k\, n_k \tag{2.1}$$

and represents the total mass in the distribution. Substitution of Eq. (1.4) into the expression for M_1 leaves

$$M_1 \sim t^{-w} \sum_{k=1}^{\infty} k^{1-\tau} f(k/t^z) \tag{2.2a}$$

$$\sim t^{-w} \int_1^{\infty} k^{1-\tau} f(k/t^z)\,dk \ . \tag{2.2b}$$

If we require the total mass to be conserved, i.e. M_1 to remain constant, then the integral in expression (2.2b) must diverge as t^w as $t \to \infty$. This happens for $\tau < 2$.[6] By a change of variables, Eq. (2.2b) can be written as

$$M_1 \sim t^{-w}\, t^{(2-\tau)z} \int_{t^{-z}}^{\infty} x^{1-\tau} f(x)dx \ , \qquad (2.3)$$

where $x = k/t^z$. Because of the restriction placed on τ this integral has no divergences, therefore

$$M_1 \sim t^{-w} t^{(2-\tau)z} \ . \qquad (2.4)$$

From the assumption that cluster mass is conserved,

$$w = (2 - \tau)z \ . \qquad (2.5)$$

The zeroth moment for any distribution is defined by

$$M_o(t) = \sum_{k=1}^{\infty} n_k(t) \qquad (2.6)$$

and represents the total number of clusters at a time t. Substitution of Eq. (1.4) into the expression for $M_o(t)$ leaves

$$M_o(t) \sim t^{-w} \sum_{k=1}^{\infty} k^{-\tau} f(k/t^z) \ . \qquad (2.7)$$

Rewriting the sum as an integral

$$M_o(t) \sim t^{-w} t^{(1-\tau)z} \int_{t^{-z}}^{\infty} x^{-\tau} f(x)dx \ , \qquad (2.8)$$

where $x = k/t^z$. This integral is finite and constant in the limit as $t \to \infty$ for $\tau \leq 1$ and $M_o(t)$ is calculated to equal

$$M_o(t) \sim t^{-z} , \tag{2.9}$$

where the exponent identity $w = (2 - \tau)z$ was used. Therefore, for $\tau \leq 1$ the total number of clusters behaves as a power law with time where the exponent z characterizes the rate of change. Since the aggregation is irreversible, we restrict $z > 0$ so that the total number of clusters decreases with time.

For the case where $\tau > 1$, the integral in Eq. (2.8) diverges at the lower limit so the first term in the sum, Eq. (2.7), is sufficient for determining the asymptotic behavior of $M_o(t)$.[6] Hence,

$$M_o(t) \sim t^{-w} \tag{2.10}$$

where $\tau > 1$ and $w > 0$. One can see from this discussion that the asymptotic behavior of the zeroth moment, i.e. the cluster population, is dependent on the value of τ.[6]

In general, the Nth moment of Eq. (1.4) is given by

$$M_N \sim t^{-w}\, t^{(N-\tau-1)} \int_{t^{-z}}^{\infty} x^{N-\tau} f(x)dx . \tag{2.11}$$

This integral has no divergences provided $N \geq 1$ and $\tau < 2$.

Therefore, the Nth moment of the scaling Ansatz behaves in a general way

$$M_N \sim t^{(N-1)z} \quad . \tag{2.12}$$

where $N \geq 1$. Thus we see asymptotic moments of first or higher order obey a dynamic scaling relation characterized by the exponent z.

Mathematically, the shape of a distribution is fixed if the relative normalized moments are constants. The relative normalized Nth moment is defined by

$$\bar{M}_N \equiv \frac{M_N/M_o}{(M_1/M_o)^N} = M_o^{N-1} \, M_N \quad . \tag{2.13}$$

For simplicity, we will assume $\tau \leq 1$. Under these conditions M_N is given by the scaling relation

$$M_N \sim t^{(N-1)z} \tag{2.12}$$

for all N. Substituting this into Eq. (2.13) leaves

$$\bar{M}_N \sim t^{-z(N-1)} t^{(N-1)z} \quad . \tag{2.14}$$

Thus we see that the relative normalized moments are not functions of time. This is expected since scaling distributions imply an unchanging shape.

Before concluding the disussion on the behavior of the moments from the scaling Ansatz, I will re-emphasize that cluster distributions scale when their shapes are fixed, i.e. their relative normalized moments are constants, and their moments scale with a power law in time characterized by the exponent z.

B. The Kinetics of Aggregation

Irreversible aggregation can be accurately described by Smoluchowski's equation in the mean field limit where thermodynamic fluctuations are unimportant. The rate of change in the number of clusters consisting of k monomers is given by

$$\dot{n}_k(t) = 1/2 \sum_{j=1}^{k-1} K_{k-j,j}\, n_{k-j}(t)\, n_j(t) - n_k(t) \sum_{j=1}^{\infty} K_{k,j}\, n_j(t) \quad . \quad (2.15)$$

The first sum on the right-hand side represents a gain in the number of clusters of mass k, resulting from a j-mer colliding with a (k-j)-mer to form a k-mer. The second sum represents a loss in the number of clusters of mass k, resulting from a j-mer colliding with a k-mer. $K_{i,j}$ is a collision kernel and is proportional to the probability of an i-mer and j-mer reacting.

The three most commonly used collision kernels for describing aggregation processes are of the general functional forms:

$$K_{i,j} = A(ij)^{\omega} \qquad \text{Product kernel}$$

$$K_{i,j} = B(i+j)^{\omega} \qquad \text{Sum kernel}$$

$$K_{i,j} = C(i^{1/d_f} + j^{1/d_f})(i^{-1/d_f} + j^{-1/d_f}) \qquad \text{Brownian kernel.}$$

Cluster distributions satisfying Smoluchowski's equation depend on the functional forms of the collision kernels. As it turns out, exact solutions to this equation exist only for the bilinear kernel[7]

$$K_{i,j} = Aij + B(i+j) + C \; . \qquad (2.16)$$

Our interests lie in the scaling form of cluster distributions, therefore asymptotic solutions to Smoluchowski's equation are more relevant here. Asymptotic solutions have been found and their forms resemble the scaling Ansatz proposed by Vicsek and Family.[7] One asymptotic solution in particular will be discussed in the next section.

The asymptotic form of the collision kernel $K_{i,j}$ has three defining exponents, υ, μ, and λ. The exponent μ is used to define three distinct aggregation classes. It will be discussed below. The exponent λ is the kernel homogeneity and it relates the aggregation kinetics to the exponents w, τ, and z from the scaling Ansatz. The relation between λ and z is general and it will be given shortly. I wish to emphasize that the relation between λ and z is important here because the moments from the Ansatz scale with

the exponent z and moments characterize distributions [see Eq. (2.12)]. Therefore, the aggregation kinetics may be used to characterize distributions.

Von Dongen and Ernst used 'self-consistency' arguments to arrive at asymptotic forms for the collision kernels.[7] They argue that because the number of active sites on a cluster cannot grow faster than its size, the reaction rates are bounded, as $j \to \infty$, by

$$\frac{K_{i,j}}{j} \leq C(i) \ , \tag{2.17}$$

where C(i) is a constant dependent on i and

$$\frac{K_{i,j}}{j^2} \leq c' \ , \tag{2.18}$$

where $i \to j$ and c' is some constant. Further, the asymptotic forms of the collision kernels are restricted to homogeneous functions for large i and/or j with the properties

$$K_{ai,aj} = a^{\lambda} K_{i,j} = a^{\lambda} K_{j,i} \ , \tag{2.19}$$

where λ is the kernel homogeneity and

$$K_{i,j} \sim i^{\mu} j^{\nu} \tag{2.20}$$

for $j >> i$. From Eq. (2.19) it follows that

$$\mu + \upsilon = \lambda \ . \qquad (2.21)$$

These restrictions can be justified in the following ways. First, the assumption that asymptotic kernels be homogeneous functions is sound since all physically relevant situations can be described with them.[8] Second, the asymptotic form of the kernel given in Eq. (2.20) is the most general for $j >> i$.

By substituting Eq. (2.20) into Eq. (2.18) we find

$$j^{\upsilon-1} \lesssim C'(i) \quad , \qquad j \to \infty \qquad (2.23)$$

where $C'(i) = C(i)i^{-\mu}$. This expression implies that $\upsilon \lesssim 1$. By substituting Eq. (2.23) into Eq. (2.21) we find

$$\frac{j^{\upsilon+\mu}}{j^2} < c' \quad , \qquad j \to \infty \qquad (2.26)$$

as $i \to j$. Thus we see that $\lambda \lesssim 2$.

The exponent μ has no restrictions placed on it so three aggregation classes have been defined:[7]

$\mu > 0$ class I kernel

$\mu = 0$ class II kernel

$\mu < 0$ class III kernel .

The asymptotic form for the collision kernel [see Eq. (2.20)] shows that for $\mu > 0$ the aggregation rate is dominated by large cluster - large cluster interactions and for $\mu < 0$ the aggregation rate is

dominated by small cluster - large cluster interactions. There is no dominant interaction characterizing class II aggregation rates.

The general relationship between the homogeneity λ and the dynamic exponent z is given by[9]

$$z = 1/(1-\lambda) \ . \tag{2.24}$$

Recall, in the introduction we found that because the cluster population decreases for irreversible aggregation processes, $z > 0$. This condition further restricts the homogeneity to $\lambda \leq 1$.

C. A Possible Solution

By arguing the most probable distribution for a cluster-cluster aggregation process, Botet and Jullien[10] arrived at the asymptotic distribution

$$n_k \sim (M_o^2/M_1)g(x) \ , \tag{2.25}$$

where

$$g(x) = \frac{(1-\lambda)^{1-\lambda}}{\Gamma(1-\lambda)} x^{-\lambda} e^{-(1-\lambda)x} \ . \tag{2.26}$$

$\Gamma(x)$ is the gamma function, λ is the kernel homogeneity and $x = M_o k/M_1$. If the B-J distribution is a scaling distribution for irreversible aggregation, then it should have the same scaling form as the Vicsek and Family scaling Ansatz.

Recall the scaling Ansatz given in Eq. (1.4) as

$$n_k \sim t^{-w} k^{-\tau} f(k/t^z) \ . \qquad (1.4)$$

This scaling distribution may be expressed in the equivalent form

$$n_k \sim s^{-\theta} \Phi(k/s) \ , \qquad (2.27)$$

where s is the mass weighted mean cluster size of a distribution defined by

$$s = \frac{\sum_{k=1}^{\infty} k^2 n_k}{\sum_{k=1}^{\infty} k\, n_k} = M_2/M_1 \qquad (2.28)$$

and $\Phi(x)$ is the cutoff function with the asymptotic limits

$$\Phi(x) \ll 1 \quad \text{for} \quad x \gg 1 \qquad (2.29a)$$

and

$$\Phi(x) \sim x^{\beta} \quad \text{for} \quad x \ll 1 \ , \qquad (2.29b)$$

where $x = k/s$.

To see the equivalence between the scaling expression in Eq. (1.4) and the one given by Eq. (2.27), assume $x \ll 1$ and substitute Eq. (2.29b) into Eq. (2.27). This will result in

$$n_k \sim t^{-(\theta+\beta)}\ k^{\beta} \tag{2.30}$$

where $s \sim t^z$ for $x \ll 1$. This expression is equivalent to the original Ansatz in Eq. (1.4) provided $\beta = -\tau$ and $\theta = 2$. Therefore,

$$n_k \sim s^{-2}\ \phi(k/s) \tag{2.31}$$

is an alternative expression for the scaling form in Eq. (1.4).

The mean cluster size for a distribution is defined by

$$\bar{s} = \frac{\sum_{k=1}^{\infty} k\, n_k}{\sum_{k=1}^{\infty} n_k} = M_1/M_0 \ . \tag{2.32}$$

Using the definition for the mean cluster size, the B-J distribution can be written as

$$n_k \sim \bar{s}^{-2} g(x) \ . \tag{2.33}$$

Here we make the assumption that the mean cluster and mass weighted cluster sizes are equivalent, i.e. assume $\bar{s} \sim t^z$ for $x \ll 1$. With this, the B-J distribution has the same scaling form as Eq. (2.27) provided the cutoff function $g(x)$ has the same asymptotic limits as $\Phi(x)$ given in Eqs. (2.29a) and (2.29b).

Recall the cutoff function from the B-J distribution

$$g(x) = \frac{(1-\lambda)^{1-\lambda}}{\Gamma(1-\lambda)}\ x^{-\lambda}\ e^{-(1-\lambda)x} \ . \tag{2.34}$$

For $x >> 1$ we have $g(x) << 1$ which agrees with Eq. (2.29a). For $x << 1$ we have $g(x) \sim x^{-\lambda}$ which disagrees with Eq. (2.29b) unless $\lambda = \tau$. The homogeniety λ is not always equal to the exponent τ for $x << 1$. We use this reason along with the ambiguity in the scaling nature of the zeroth moment, $\bar{s}$, to conclude that the B-J distribution does not scale in accordance with the Vicsek and Family Ansatz for $x << 1$. For $x >> 1$, however, it does.

The B-J distribution was used for calculating intensity-weighted moments. Although the B-J distribution has ambiguous scaling properties for $k/t^z << 1$, hence an inexact scaled cluster distribution, we justify its exactness for calculating intensity-weighted, scaled moments with the following argument.[11]

For simplicity the argument is restricted to the Rayleigh limit where the scattered intensity from a cluster goes as its mass squared. In the Rayleigh limit, the second moment of a cluster distribution represents the total scattered intensity, i.e.

$$M_2 \simeq \int_k k^2 n_k dk \ , \qquad (2.35)$$

where $k^2 \alpha I_k$. I_k is the scattered intensity from a cluster of mass k. The dominant contributions to this integral come from those clusters with a large mass, k. Because the B-J distribution was used to calculate intensity-weighted moments, the small mass end of this scaling distribution where $k/t^z << 1$ was dominated by its large mass end where $k/t^z >> 1$. Therefore, the scaling inconsistencies at the

small mass end of the distribution did not affect the accuracy in the intensity-weighted, scaled moments calculated from this distribution. Whether or not the B-J distribution is a good approximate solution for the Smoluchowski equation remains to be tested experimentally.

We find the N-th moment of the B-J distribution by multiplying Eq. (2.25) by k^N and summing over all k. The result is

$$M_N \sim \frac{\Gamma(N + 1-\lambda)}{\Gamma(1-\lambda)} \left[\frac{M_1}{1-\lambda}\right]^N M_o(t)^{1-N} \quad . \tag{2.36}$$

Notice that the time dependence of the N-th moment enters in only through M_o.

D. Dynamic Light-Scattering and Its Moments

Consider a system made up of two k-mers fixed in space with a laser beam focussed onto them. Assume k-mer one and two are isotropic scatterers. Therefore, the scattered light is of equal intensity in all directions. Somewhere off at infinity relative to the volume occupied by the two k-mers, will be a stationary, superimposed Fraunhofer intensity pattern. This interference pattern is characterized by the relative separation between the two k-mers. Set the k-mers into motion. The superimposed Fraunhofer pattern will now fluctuate as a result of the changing relative separations between k-mers one and two.

The dynamic light scattering technique, photon correlation spectroscopy, is used to correlate the scattered intensity fluctuations resulting from diffusing Brownian k-mers.[12] The net result is a measured intensity autocorrelation function given by

$$\langle I(t) \cdot I(t+\tau) \rangle \ . \tag{2.37}$$

The brackets represent a time average or equivalently an ensemble average. τ is defined as a sample time and it represents a distance between intensity fluctuations. The autocorrelation function is independent of any initial time, therefore

$$\langle I(t) \cdot I(t+\tau) \rangle = \langle I(0) \cdot I(\tau) \rangle \ . \tag{2.38}$$

For a monodisperse system of scatterers the intensity autocorrelation function has a purely exponential form that is given by

$$C(t) \equiv \langle I(0) \cdot I(\tau) \rangle = Ae^{-2\Gamma t} + B \ . \tag{2.39}$$

This equation is illustrated in Figure 2.1. B represents an experimentally determined background and A is the amplitude of the autocorrelation function determined with the signal-to-noise ratio, S/N by

$$A = (S/N) \cdot B \ . \tag{2.40}$$

The linewidth Γ is related to the correlation time τ_c by

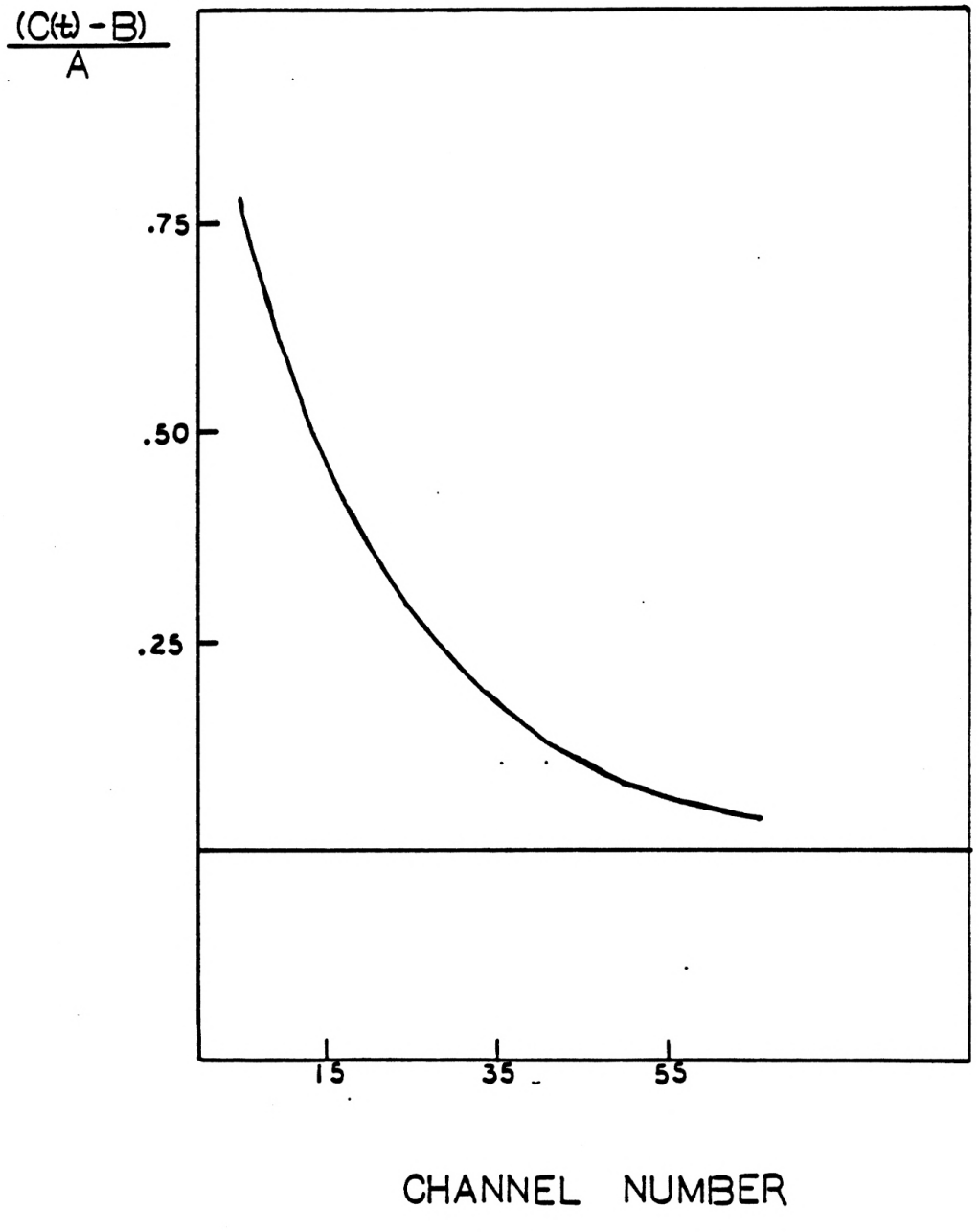

Fig. 2.1 The autocorrelation function for a monodisperse sol is a pure exponential. Here, the time is measured in channel numbers so the correlation function has the form

$$(C(t) - B)/A = e^{-2\Gamma n\tau} ,$$

where n is a channel number and τ is a sample time. $\Gamma = 2500\ \text{sec}^{-1}$ and $\tau = 10\ \mu\text{sec}$.

$$\Gamma = 1/(2\ \tau_c)\ . \qquad (2.41)$$

The correlation time indicates how fast the correlation function decays. The rate of decay is directly proportional to the rate at which the scatterers are diffusing, i.e.,

$$\tau_c = (2Dq^2)^{-1}\ . \qquad (2.42)$$

Here, D is the appropriate diffusion constant and q is the scattered wavevector given by

$$q = (4\pi/\lambda)\ \sin\ \theta/2\ . \qquad (2.43)$$

In the expression for q, λ represents the wavelength of light in the scattering volume and θ is the scattering angle.

Real systems are polydisperse and the intensity autocorrelation function deviates from any purely exponential form. Using the method of cumulants,[13] the autocorrelation function is commonly fit to a function of the form,

$$g(t) = A\exp\left[2\ \sum_{n=1}^{\infty}(-1)^n\mu_n t^n/n!\right] \qquad (2.44)$$

where the μ_n's are the cumulants and $g(t) = C(t) - B$. Only the first two cumulants will be considered here.

The first cumulant μ_1 is an average linewidth given by

$$\mu_1 = \langle\Gamma\rangle\ , \qquad (2.45)$$

where

$$\langle \Gamma \rangle = \int_{\Gamma} \Gamma G(\Gamma) d\Gamma \ . \qquad (2.46)$$

This expression tells us that $\langle \Gamma \rangle$ is the first moment of the linewidth distribution $G(\Gamma)$. Clusters with different radii have different decay rates, hence a polydisperse system of clusters must have a distribution of linewidths. It is well known that the linewidth distribution is related to the cluster distribution by

$$G(\Gamma)\ d\Gamma = I_k n_k dk \ , \qquad (2.47)$$

where I_k is the total scattered intensity from a cluster of mass k. With this relation one can show that Γ is an intensity weighted moment of the cluster distribution.

We restrict ourselves to the Rayleigh limit where the scattered intensity goes as the mass squared, i.e.

$$I_k \sim k^2 \ . \qquad (2.48)$$

Recall from Eq. (2.42) that Γ is proportional to the diffusion constant D. In the hydrodynamic limit

$$D \sim 1/R_H \ , \qquad (2.49)$$

where R_H is the hydrodynamic radius of a cluster. For a self-similar cluster, the cluster volume is related to its radius of gyration by

$$k \sim R_g^{d_f} \ , \qquad (1.3)$$

implying

$$R_g \sim k^{1/d_f} . \tag{2.50}$$

In recent work discussing the hydrodynamic behavior of self-similar clusters, Wiltzius[14] showed the ratio R_H/R_G to remain constant for the cluster size range of $500\text{Å} \leq R_H \leq 7000\text{Å}$. With this we can write Eq. (2.50) as

$$R_H \sim (1/k)^{1/d_f} \tag{2.51}$$

and Γ as

$$\Gamma \sim (1/k)^{1/d_f} . \tag{2.52}$$

Substituting Eqs. (2.47), (2.48), and (2.52) into Eq. (2.46) we arrive at

$$\langle\Gamma\rangle \sim \int (1/k)^{1/d_f} k^2 N_k \, dk \tag{2.53}$$

or

$$\langle\Gamma\rangle \sim M_{2-1/d_f} . \tag{2.54}$$

$\langle\Gamma\rangle$ is an intensity weighted moment of the cluster distribution and greater than one since the lower bound on a fractal dimension is one. Therefore, we expect $\langle\Gamma\rangle$ to scale with time as a power law characterized by the exponent z once the cluster distribution has scaled [see Eq. (2.13)].

The second cumulant μ_2 is a measure of the correlation function's deviation from a purely exponential form [see Fig. 2.2]. μ_2 is given by

$$\mu_2 = \langle \Gamma^2 \rangle - \langle \Gamma \rangle^2 \ . \tag{2.55}$$

Quite often a polydispersity index Q is defined and used as a relative measure for determining the width of a cluster distribution. It is defined by

$$Q \equiv \mu_2/\mu_1^2 = \frac{\langle \Gamma^2 \rangle}{\langle \Gamma \rangle^2} - 1 \ . \tag{2.56}$$

Notice that Q is an intensity weighted relative normalized moment. Using Eqs. (2.53) and (2.54), Q can be expressed in terms of the cluster distribution's moments as

$$Q = \frac{M_{2-2/d_f} \ M_2}{(M_{2-1/d_f})^2} \ . \tag{2.57}$$

Sorensen and Taylor[15] have suggested using the moments from the asymptotic B-J distribution, Eq. (2.25), to evaluate the moments in this expression for Q. Using the general expression for the B-J moments in Eq. (2.36), one arives at

$$Q_\infty = \frac{\Gamma(3-\lambda-2/d_f)\ \Gamma(3-\lambda)}{[\Gamma(3-\lambda-1/d_f)]^2} \ . \tag{2.58}$$

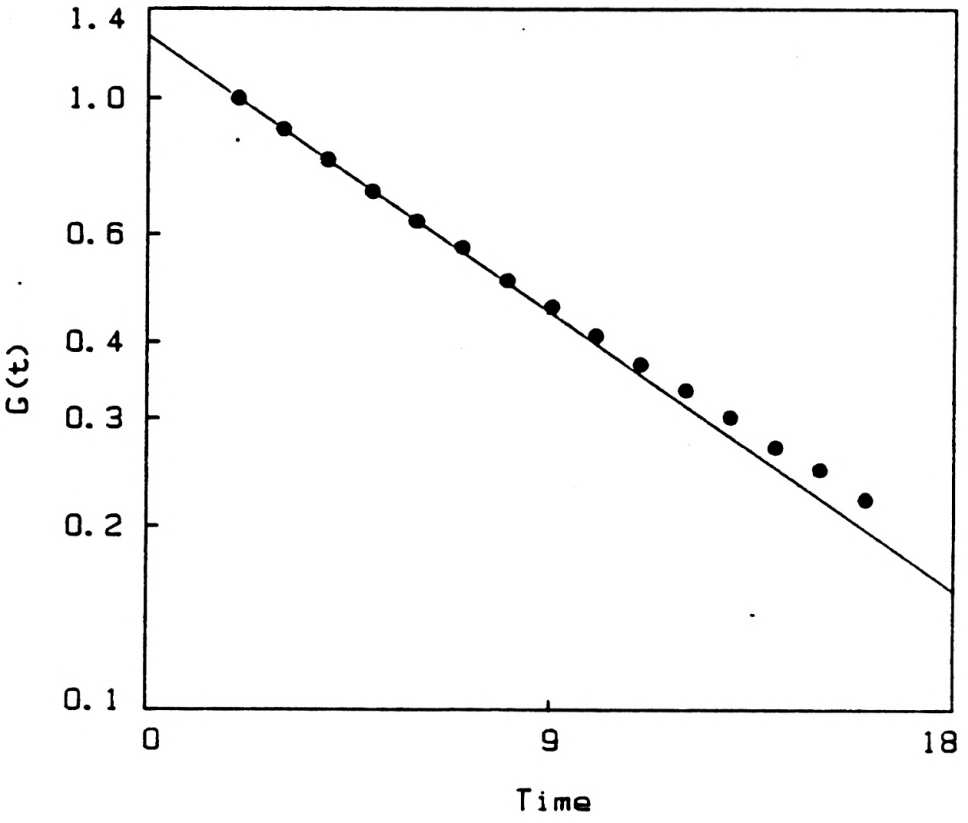

Fig. 2.2 Actual data from a well aggregated sol. The experimental data was fit with the first two cumulants so the autocorrelation function was assumed to have the form

$$g(n\tau) = Ae^{-2\mu_1 n\tau + \mu_2(n\tau)^2} .$$

To measure the effect of the second cumulant μ_2 we take the natural logarithm of each side of the above equation, yielding

$$\ell n[g(n\tau)] = -2\mu_1 n\tau + \mu_2(n\tau)^2 + \ell nA .$$

From this equation one sees that linearity is lost, on a semi-log plot, when μ_2 is significant. A contributing μ_2 implies a polydisperse sol and the autocorrelation function is no longer purely exponential. For the well aggregated sol, μ_2 is significant.

This asymptotic expression for Q is independent of time, expected since Q is a relative normalized moment, and a function of the kernel homogeneity and fractal dimension of the clusters [see Fig. 2.3)]. Since Q_∞ is independent of time, we expect it to evolve from some arbitrary initial value to a final constant one. Recall that constant relative normalized moments imply scaling distributions. Therefore, the evolution of Q into some final asymptotic value implies the cluster distribution has evolved into a final scaling form.

E. Two Distinct Aggregation Regimes

Weitz et al.[16,17] have shown that two distinct regions of growth exist for aggregating gold colloids. They are the reaction-limited and diffusion-limited aggregation regimes, RLA and DLA respectively. In the reaction-limited regime, the reaction rate is controlled by the reaction time between the bonding clusters. In other words, the reaction time is the rate determining step in the aggregation process. For RLA, the cluster radii have been found to grow exponentially in time.[17] Since the first cumulant is proportional to the inverse average cluster radius, we express this growth law as

$$\langle\Gamma(0)\rangle/\langle\Gamma(t)\rangle \sim e^{ct} . \qquad (2.59)$$

Exponential growth implies reaction-limited aggregation, but reaction limited aggregation does not have to imply exponential

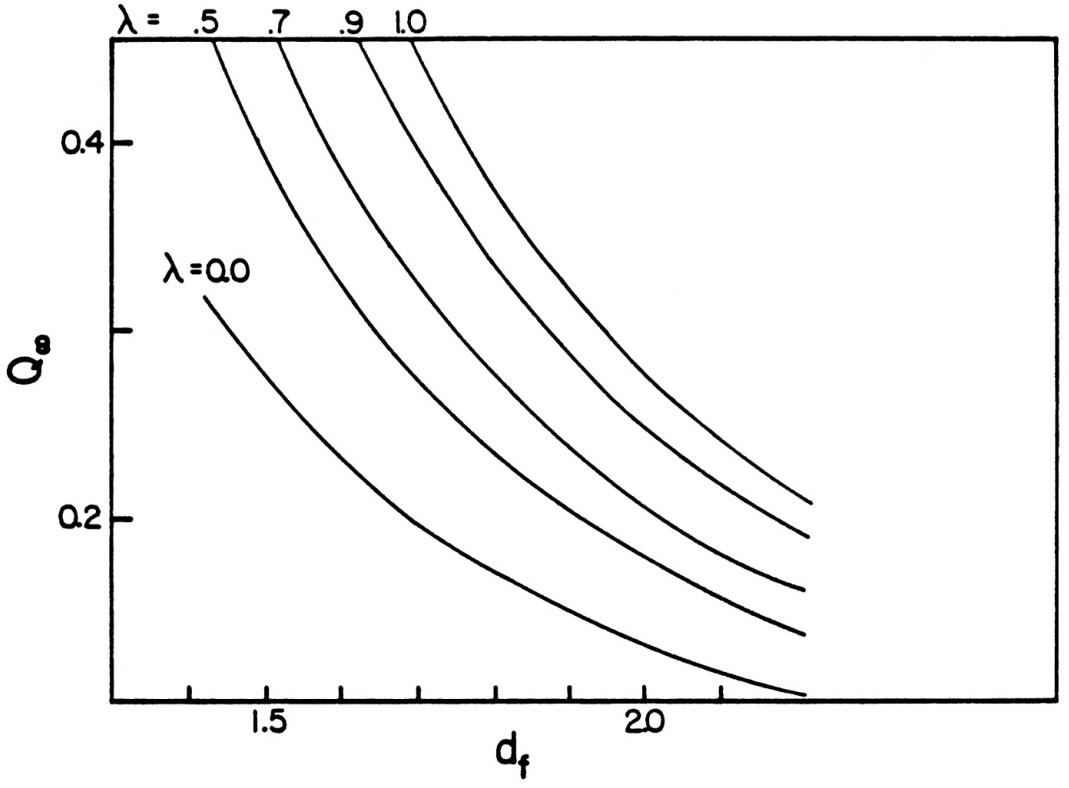

Fig. 2.3 A plot of the asymptotic values of Q vs. the fractal dimension of the aggregated clusters. Each curve represents a different kernel homogeneity, λ. The values Q_∞ are predicted by the B-J scaling distribution.

growth. In the diffusion-limited aggregation regime, the diffusing rate of the cluster is the rate determining step in the aggregation process. For the DLA process the cluster radii exhibit power law growth,[16]

$$\langle\Gamma(0)\rangle/\langle\Gamma(t)\rangle \sim t^{1/d_f} . \tag{2.60}$$

Recall the expression for the first cumulant in terms of a moment,

$$\langle\Gamma\rangle \sim M_{2-1/d_f} . \tag{2.54}$$

This moment scales according to Eq. (2.12); therefore,

$$\langle\Gamma\rangle \sim t^{-z/d_f} \tag{2.61}$$

where Γ was normalized with respect to the total scattered intensity M_2. Comparing this expression with the one for growth in the diffusion-limited regime, Eq. (2.60), one finds $z = 1$. From Eq. (2.24) where $z = 1/(1-\lambda)$ we see that for DLA the homogeneity λ is found to be zero. Diffusion-limited aggregation does not have to imply a kernel homogeneity equal to zero.

CHAPTER III

Experiment

A gold solution was made using the procedure of Turkevich.[18] The steps in the procedure are the following:

1) Boil 212.5cc of H_2O
2) Add 25cc of 0.1% $HAuCl_4 \cdot 3H_2O$ (by wt)
3) Wait for the solution to boil again
4) Add 12.5cc of 1.0% $Na_3\ C_6H_5O_7 \cdot 2H_2O$ [sodium citrate] (by wt)
5) Let the solution boil for an additional 30 min.
6) Remove the solution from the heat and let it cool to room temperature.

For the entire duration of the heating, the solution is continuously stirred. The cloroauric acid (HAu $C\ell_4 \cdot 3H_2O$) was from Aldrich Chemicals.

Two comments concerning the preparation are necessary. First, all glassware being used must be scrupulously cleaned. All glassware that came into contact with the reduced gold solution was rinsed with a dilute aqua regia solution, boiled in a dilute nitric acid solution, rinsed with a 0.7M hydrofluoric acid solution and thoroughly flushed with purified water. All other glassware was rinsed with a 0.7M solution of HF before being flushed with purified water. Second, all the water being used for making up the chloroauric acid solution ($HAuCl_4$), the sodium citrate solution ($Na_3C_6H_5O_7$), and the gold sol was purified. Purified water was

distilled, deionized through an ion exchange resin, then pushed through a 0.22 μ pore filter. The filters were MF-Millipore filters, type GS. These type filters have a cellulose acetate and nitrate membrane which is hydrophilic and will not suffer damages from dilute acid solutions. This will become important later. Before doing any serious filtering, at least one liter of water was pushed through a new filter to leach away any surfactant. I cannot overemphasize the important role of cleanliness for producing a monodisperse system of gold monomers.

The chemistry involved during the reduction of the gold is interesting and a model describing the reduction will be proposed here.[19] The chloroauric acid solution consists of hydrogen ions, H^+, and chloroaurate ions, $AuCl_4^-$. When the sodium citrate solution is introduced, the chloroaurate ions dissociate and the auric ions, Au^{+3}, are reduced by the carboxylate groups located on the citrate ions (see Fig. 3.1a). The remaining citrate ions behave as weak ligands and attach themselves to the reduced gold particles. A most general definition for a ligand is a molecule with the ability to donate electron pairs when bonding. The citrate ions have a net negative charge on them, thereby accounting for the stability of the colloid. TEM micrographs show these particles are spherical with an average radius of 15 nm (see Fig. 3.2).

Once the reaction was completed and the colloidal gold suspension had cooled to room temperature, a portion was filtered off through a 0.22μ pore filter into a scattering cell. The filter

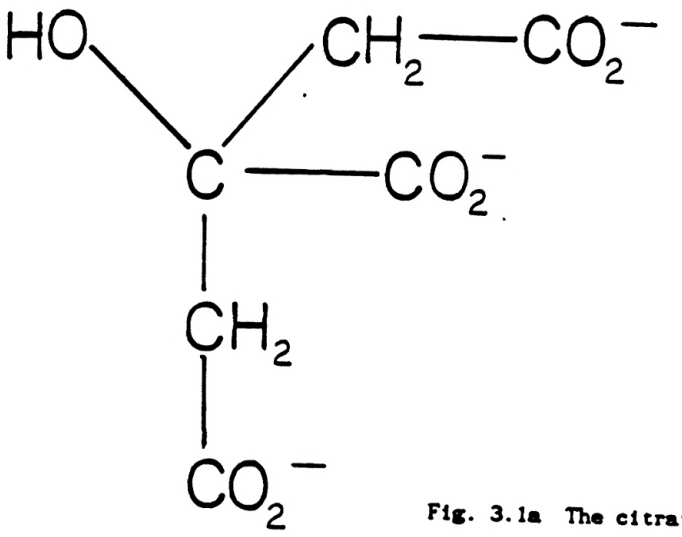

Fig. 3.1a The citrate ion.

$C_6H_5O_7^{-3}$

Fig. 3.1b The neutral pyridine molecule. Note the lone pair of electrons dangling off the nitrogen atom. This pair of electrons accounts for the molecules absorption onto the gold particle surface.

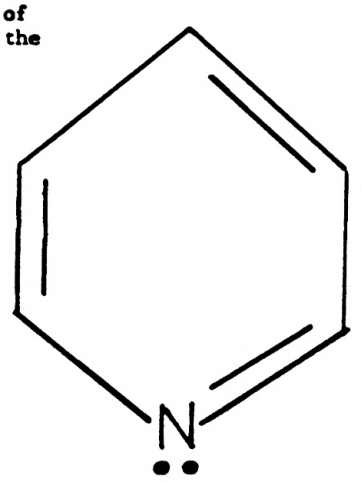

C_5H_5N

Fig. 3.2 A TEM micrograph of a typical gold sol before pyridine was introduced. Dynamic light scattering determined an average monomer radius of 15.4 nm.

used was also a type GS and here the membrane type was important. Since the reduced gold solution was slightly acidic, the membrane had to be inert to a lower pH. The scattering cell was a quartz spectrometer cell 45 mm high and 12.5 mm square with a ground glass cap. Before a coagulating agent was introduced into the cell, a few PCS spectra were taken to determine the starting conditions for the colloid. The starting conditions consisted of an average monomer radius and an initial value for Q. For five different experimental runs, the PCS spectrums taken at t = 0 revealed initial average particle diameters ranging from 18nm to 28nm and initial Q values between .04 and 0.1.

The coagulant used was pyridine (C_5H_5N). It was diluted from an original 'ultrapure' 99+% stock solution from Alpha Products. The diluting was done with purified water and any pyridine that went into gold suspensions was first filtered through a 0.22μ pore filter of type GS. It was later found out that pyridine and cellulose acetate and nitrate membrane, are not compatible. Pyridine will dissolve membranes of this nature. Fortunately, the filtered pyridine solutions were dilute, the maximum concentration was on the order of 10^{-4}M, and no visual damage to the filters was observed. The final pyridine concentrations in the gold suspensions were between 5.9×10^{-5}M and 8.6×10^{-4}M. The neutral pyridine molecule (see Fig. 3.1b) is a more effective ligand than the citrate ion, i.e. it bonds more favorably with the gold. For this reason, the

pyridine molecules are absorbed onto the surface of the gold displacing the stabilizing citrate ions, thereby initiating aggregation.

The rates of growth in our gold sols were altered by differing the amounts of pyridine concentrations needed to induce the aggregation. Physically, a varying pyridine concentration causes a varying reaction probability between the clusters. In other words, the collision kernel changes its form or homogeneity. Therefore, the collision kernels needed to represent the aggregation kinetics in our sols will depend on the final pyridine concentrations. Aggregation times ranged from 3 to 11 hours. The resulting clusters from our gold sols were open and diffuse displaying a fractal nature [see Fig. 3.3].

The experimental set-up is illustrated in Fig. 3.4. An argon ion laser was used and operated at 488 nm. The beam was focused into the quartz scattering cell with a double convex, 170 mm focal length lens. The scattering volume was focussed onto the iris of a photomultiplier tube with a double convex, 100 mm focal length lens so that the image magnification was approximately one. In front of the iris on the photomultiplier tube was a slit with a width of approximately 1 mm. The effect of the lens and slit combination in the front of the photomultiplier tube was to increase the coherence area on the tube's photocathode resulting in an optimum

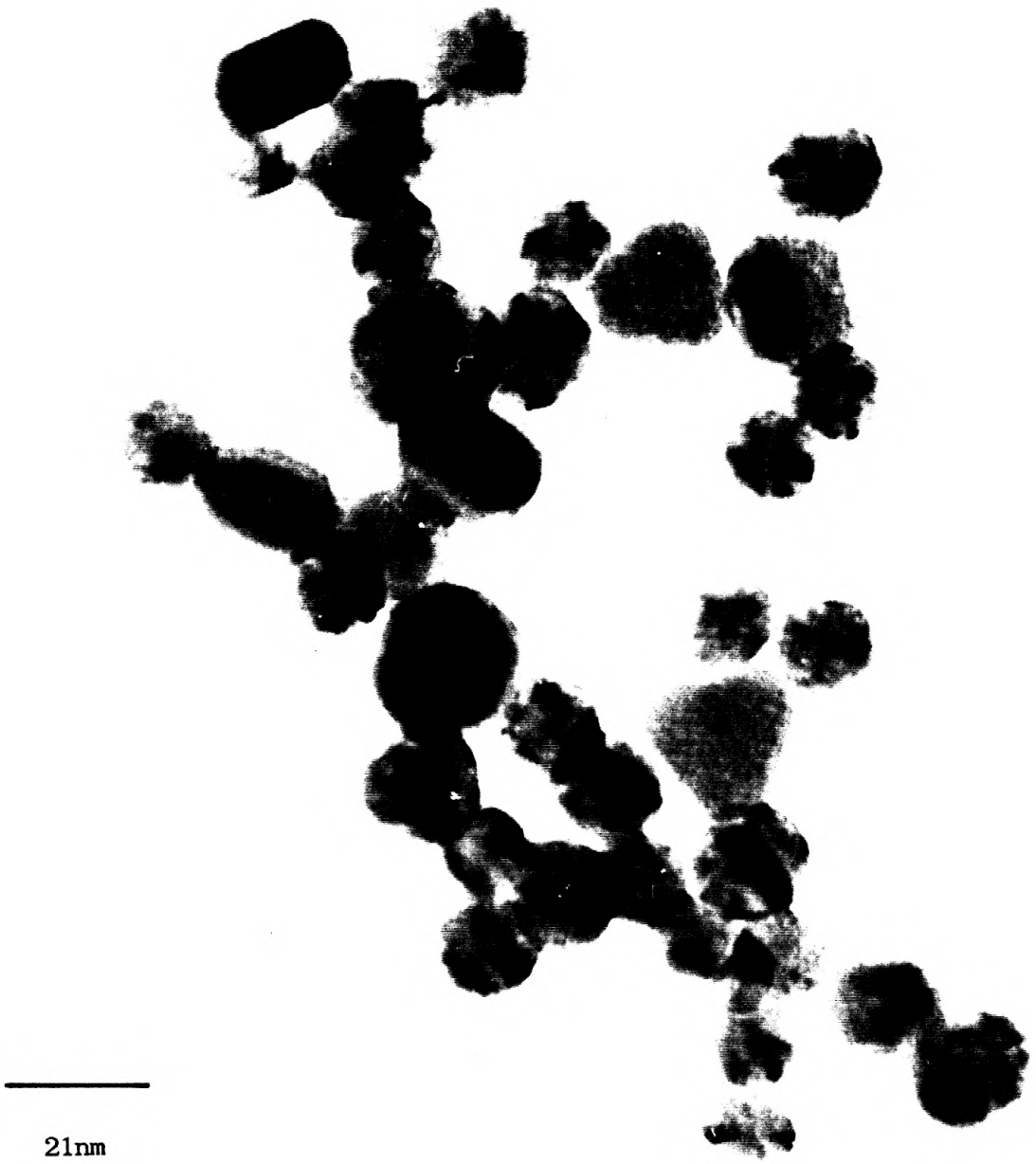

Fig. 3.3 A TEM micrograph of a typical gold sol somewhere near the end of its allowed aggregation. Dynamic light scattering determined an average cluster radius of 64 nm.

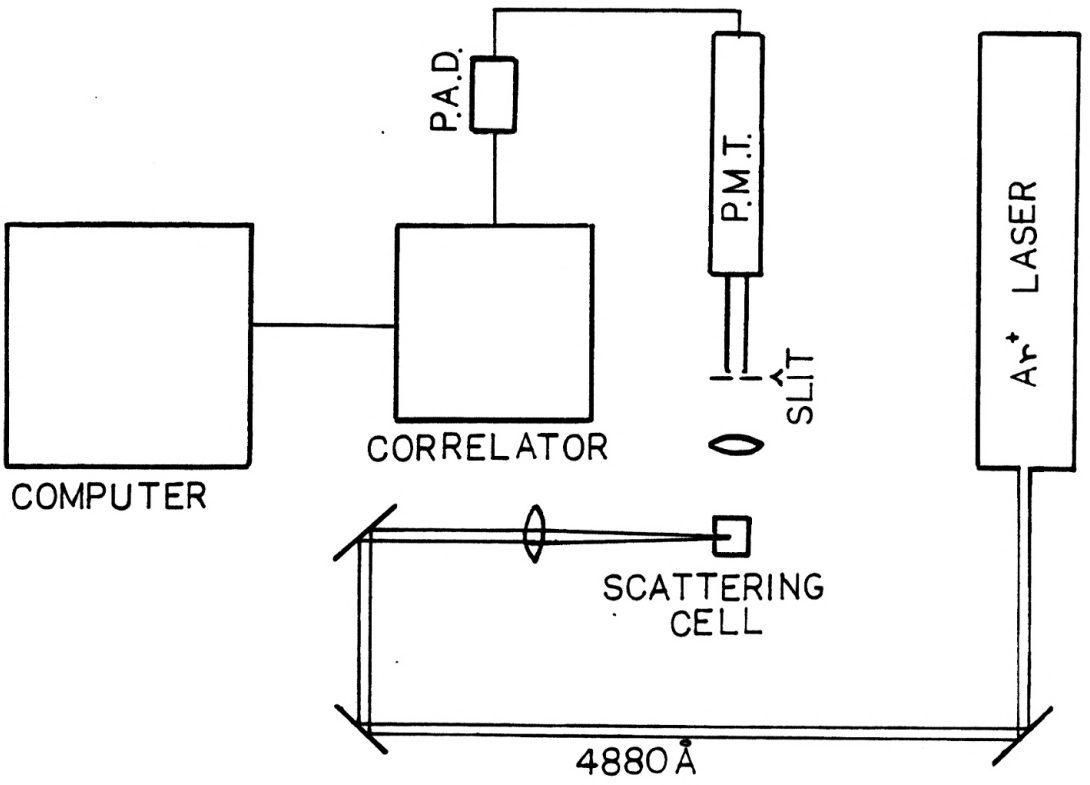

Fig. 3.4 Experimental Set-up

signal-to-noise ratio. The photomultiplier tube was a Thorn EMI model 9863A/100. It had an S20 spectral response and was designed for wide bandwidth, high gain photon counting applications. The photomultiplier tube received the scattered intensity at 90^{o} relative to the incident beam direction. The signals from the photomultiplier went into a pulse amplifier-discriminator. There the signal was amplified and sent into a digital Langley-Ford correlator, model 1096. The correlator was allowed to calculate a correlation function until the total number of counts received reached approximately 3×10^{8} counts. We have found that total counts on this order of mangitude insure good statistics, which in turn installs confidence in the calculated cumulants. The correlator then dumps the calculated correlation function onto a computer where it is stored on disk.

The intensity autocorrelation function was fit using a first and second order least squares fitting method. The autocorrelation function expressed in terms of the first two cumulants is

$$g(t) = Ae^{-2\mu_1 t + \mu_2 t^2} \tag{3.3}$$

[see Eq. (2.59)]. Taking the natural logarithm of each side results in

$$\ln g(nt) = -2\mu_1(n\tau) + \mu_2(n\tau)^2 + \ln A \tag{3.4}$$

where n represents a channel number and τ a sample time.

The first cumulant was found by first order least squares fitting the data with

$$\ln g(nt) = -2\mu_1(n\tau) + \ln A \ . \qquad (3.5)$$

The fit was done for the first 18 channels, then the first 17 channels, 16 channels, etc. down to the first 4 channels. Here, the first n channels refer to channels 2 through n. The number one channel was not considered because of afterpulsing from the photomultiplier tube. The fifteen values for μ_1, found from least squares fitting with Eq. (3.5), were then linearly extrapolated back to the origin at t = 0. The extrapolated value at the origin was taken for μ_1.

The second cumulant μ_2 was found by second order least squares fitting the data with Eq. (3.4). The number of channels used to fit Eq. (3.4) was varied until μ_1 agreed with the first cumulant found from the extrapolation technique. At this point, the corresponding value for μ_2 was taken as the second cumulant.

To guarantee a known background, the total number of counts accumulated by the correlator, while calculating an autocorrelation function, was on the order of 10^8 photon counts. This total number of counts required a real time interval of approixmately 7 minutes during which the clusters were growing. The growth of the clusters during this time interval introduced a nonstatic second cumulant μ_{ns}, which contributed to the polydispersity index Q. We show that this contribution to Q can be neglected.[11]

For approximating the contribution of μ_{ns} to Q, a log-normal cluster distribution is assumed. The average asymptotic Q value found from experiment was 0.18. The polydispersity index Q is related to the distribution width by[20]

$$Q = \exp(\ell n^2 \sigma) - 1 \ . \qquad (3.6)$$

The initial geometric width σ corresponding to an asymptotic Q of 0.18 is calculated to equal 1.5.

Cluster growth during a finite correlation time broadens a distribution [see Fig. 3.5]. By how much does the width of a log-normal cluster distribution broaden during a 7 minute correlation time inteval? The answer to this question is bounded by our fastest and slowest sol aggregation rates. Since $\langle\Gamma\rangle \propto 1/\langle R_H\rangle$,

$$\frac{d\langle\Gamma\rangle/dt}{\langle\Gamma\rangle} = \frac{d\langle R_H\rangle/dt}{\langle R_H\rangle} \ . \qquad (3.7)$$

The sol which aggregated quickest had $d\langle\Gamma\rangle/dt \simeq 0.82$ [see Fig. 3.6]. The slowest aggregated sol had $d\langle\Gamma\rangle/dt \simeq 0.19$.

The initial radius corresponding to the 1.65/e value of the log-normal distribution is

$$\sigma R_o = R_o + \Delta \ . \qquad (3.8)$$

Δ is the displacement from R_o to this radius and the peak distribution radius is related to the intensity-weighted radius by[20]

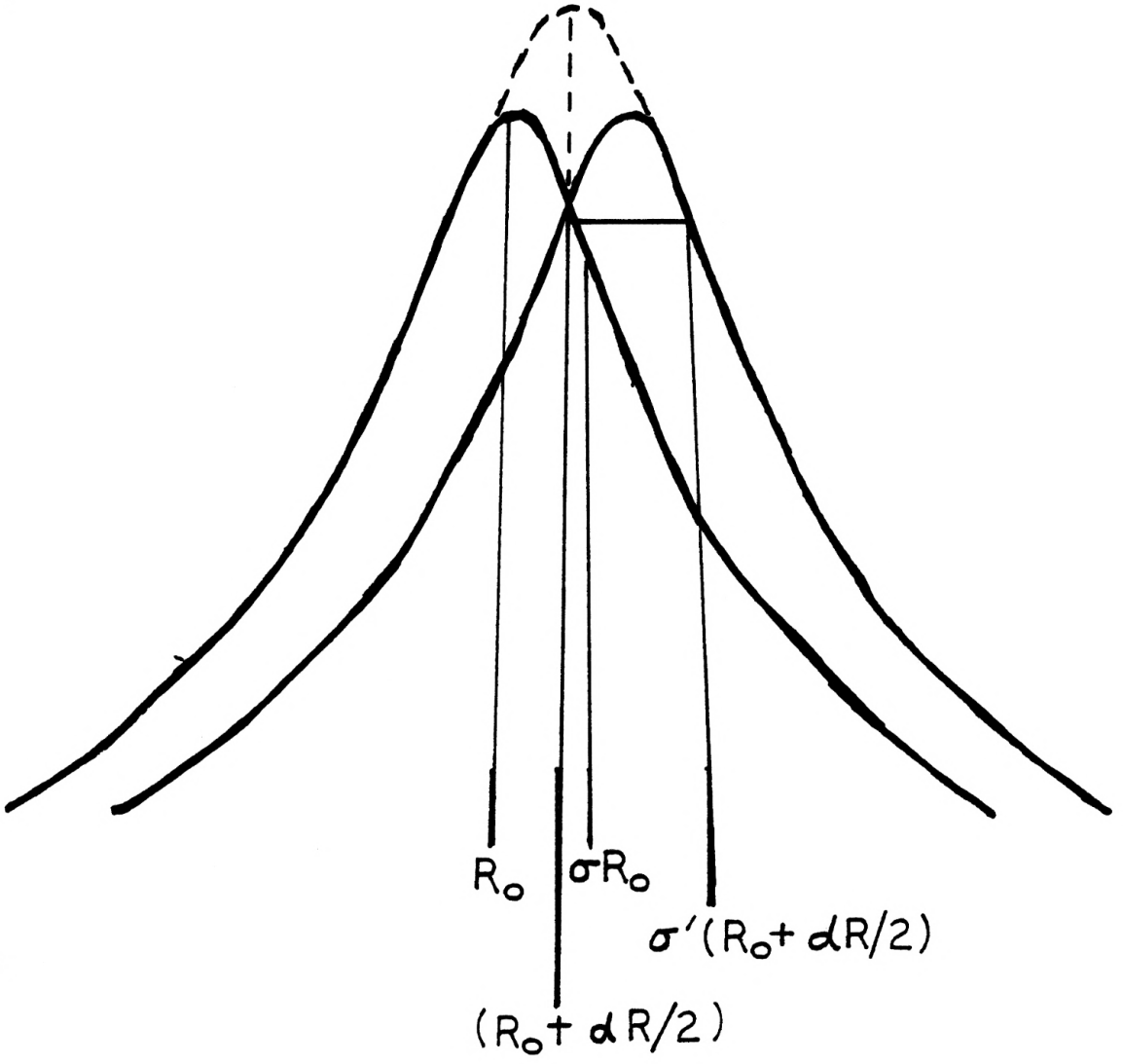

Fig. 3.5 An exaggerated schema of a propagated, scaled log-normal distribution with an initial geometric width of $\sigma = 1.5$. A finite correlation time results in an effective width σ' broader than the static one.

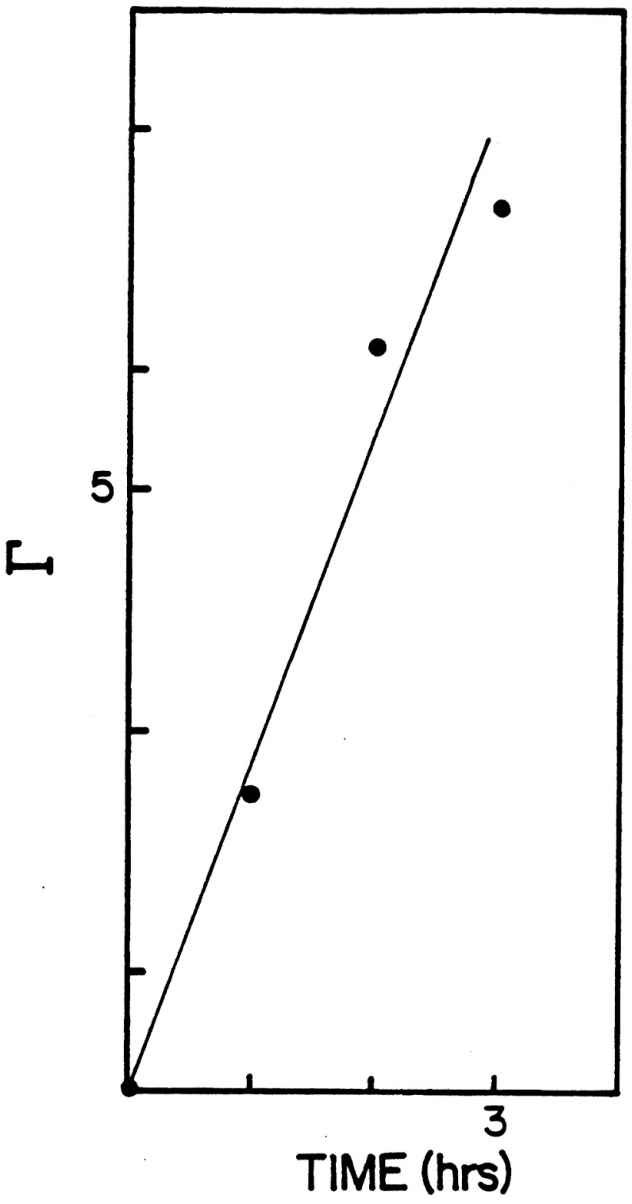

Fig. 3.6 A plot of $\langle\Gamma\rangle$ vs. aggregation time for the gold sol with the fastest cluster growth rate.

$$R_o = \langle R_H \rangle \exp\ (-6.5\ \ell n\ ^2\sigma)$$

Using Eq. (3.8) to solve for the displacement we find

$$\Delta = (\sigma - 1)\ \langle R_H \rangle \exp\ (-6.5\ \ell n^2\sigma) \qquad (3.10)$$

To calculate the spread in the log-normal distribution we calcuate the radius corresponding to the 1.65/e point after the 7 minute correlation interval, i.e.

$$\sigma'(R_o + dR/2) = R_o + \Delta + dR \qquad (3.11)$$

Using Eqs. (3.7), (3.9) and (3.10) σ' is found. Substituion of σ' into Eq. (3.6) yields a new value for Q which we denote by Q_{ns} Built into Q_{ns} is the polydispersity which resulted from the cluster growth during the finite correlation time interaval. Note that Q_{ns} is the experimentally measured value for Q and

$$Q_{ns} = Q_s + \Delta Q \qquad (3.13)$$

where Q_s is a static polydispersity index. The ΔQ's were calculated for 3 gold sols with different cluster growth rates. The results are given in Table 3.1.

Table 3.1

Sol No.	ΔQ	Growth Rate
5	.020	fastest
2	.004	intermediate
3	.001	slowest

From these results we assume the change in Q resulting from a finite correaltion time is within the experimental error of the aymptotic Q values and can therefore be neglected.

The accuracy of the cumulants was determined from the initial conditions. Three PCS spectra were taken before the coagulant pyridine was introduced in each of the five sols. The initial cumulants were analyzed from each spectrum and an experimental error was determined. We have found that $\langle\Gamma\rangle$ could be determined to an accuracy of 1.4% and Q could be determined to within $\pm$ .02 of its calculated value. These findings are quite reproducible.

CHAPTER IV

Results

A table summarizing initial, final, and relevant conditions for the five different aggregated gold sols is given below.

Table 4.1

Sol No.	$\langle R\rangle_o$ (nm)	$\langle R\rangle_f$ (nm)	Q_o	Q_∞	RoG (nm/sec)	T_∞ (hrs)	$\langle R(T_\infty)\rangle/\langle R(0)\rangle$	z/d_f from T_∞
1	9.4	38.2	.10 ±.02	.17 ±.02	1.3×10^{-3}	2.25±.25	2.2 ± .1	0.60±.02
2	9.5	68.6	.08 ±.02	.19 ±.02	2.7×10^{-3}	2.0 ±.50	3.2 ± .3	0.69±.02
3	14.7	37.8	.05 ±.02	.18 ±.02	6.1×10^{-4}	3.75±.50	1.4 ± .1	0.50±.01
4	14.8	64.0	.04 ±.02	.19 ±.02	1.6×10^{-3}	2.5 ±.50	1.7 ± .3	0.74±.01
5	14.2	67.0	.06 ±.02	.19 ±.02	4.2×10^{-3}	2.0 ±.25	2.6 ± .2	1.00±.07

The five different aggregated sols were assigned numbers 1 through 5. $\langle R\rangle_o$ and $\langle R\rangle_f$ are the initial and final average cluster radii from the five aggregated sols. Initial conditions pertained to measurements made before the addition of pyridine. Q_o is the initial value for the polydispersity index as given in Eq. (2.71) and Q_∞ is the experimentally determined asymptotic value for Q. RoG represents the rate of growth for each suspension and is defined by

$$\text{RoG} \equiv \frac{\langle R\rangle_f - \langle R\rangle_o}{(\text{allowed aggregation time})} . \qquad (4.1)$$

T_∞ is the real time interval from the onset of aggregation until Q

first appeared asymptotic. $\langle R(T_\infty)\rangle/\langle R(0)\rangle$ is the ratio of the average cluster radii where Q first appeared asymptotic divided by the initial radii. z/d_f is the slope from the full-log plots of $\langle R(t)\rangle/\langle R(0)\rangle$ against aggregation time. From the scaling Ansatz, the first cumulant should scale according to

$$\langle \Gamma \rangle \sim t^{-z/d_f} \tag{2.76}$$

or

$$\langle R(t) \rangle \sim t^{z/d_f} . \tag{4.2}$$

The slopes begin at the times where Q first appears asymptotic. These plots are illustrated in Figs. 4.1a, 4.1 b, 4.1c, 4.1d and 4.1e. Notice that they clearly indicate a power law growth after their respective asymptotic times T_∞, although the data extend for less than a decade.

Figures 4.2a, 4.2b, 4.2c, 4.2d and 4.2e are semi-log plots of the same average cluster growth against aggregation time. If the average cluster growth is exponential it will appear linear on these plots. These plots indicate possible exponential cluster growths at early times but their linearities are clearly lost at intermediate aggregation times. At these intermediate aggregation times, the cluster growths should appear power law if they are no longer exponential. This crossover from possible exponential growth to definite power law growth is confirmed by the corresponding full-log

Fig. 4.1a
Average rate of growth vs. aggregation time for sol number 1, $T_{\infty} \simeq 2$ hrs and $(z/d_f)_{T_{\infty}} \simeq .6$

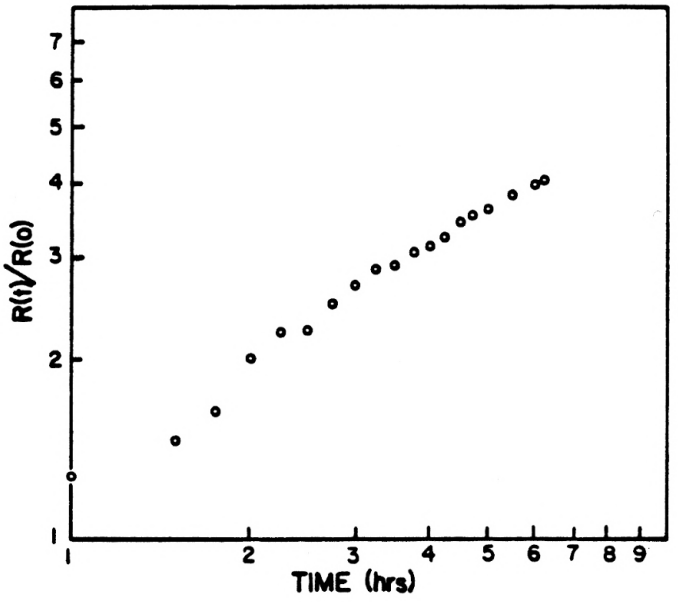

Fig. 4.2a
Average rate of growth vs. aggregation time for sol number 1.

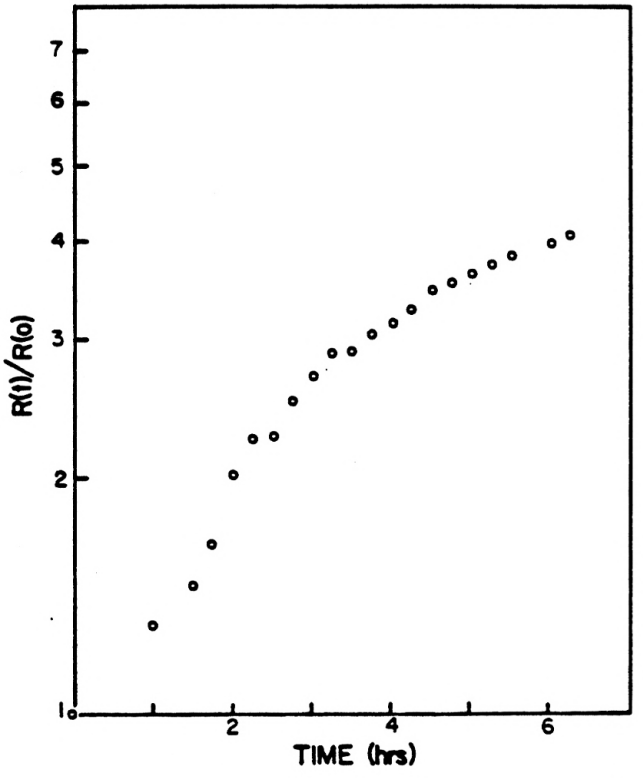

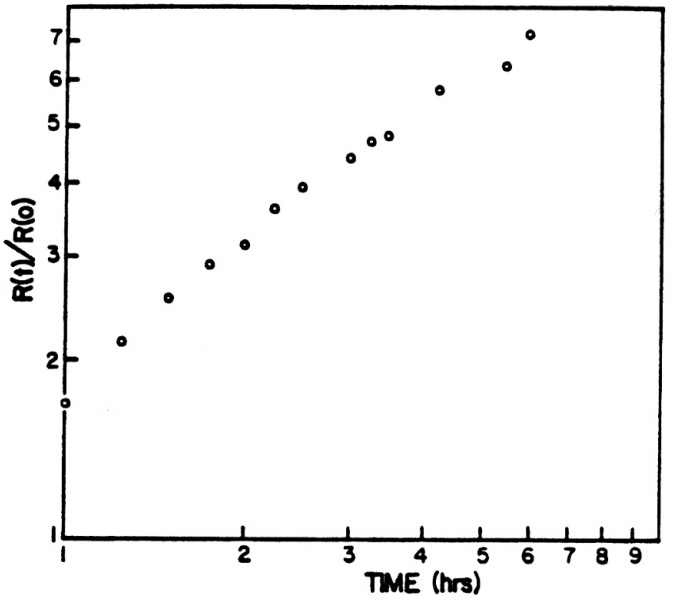

Fig. 4.1b
Average rate of growth vs. aggregation time for sol number 2. $T_\infty \approx 2$ hrs and $z/d_f)_{T_\infty} \approx .7$

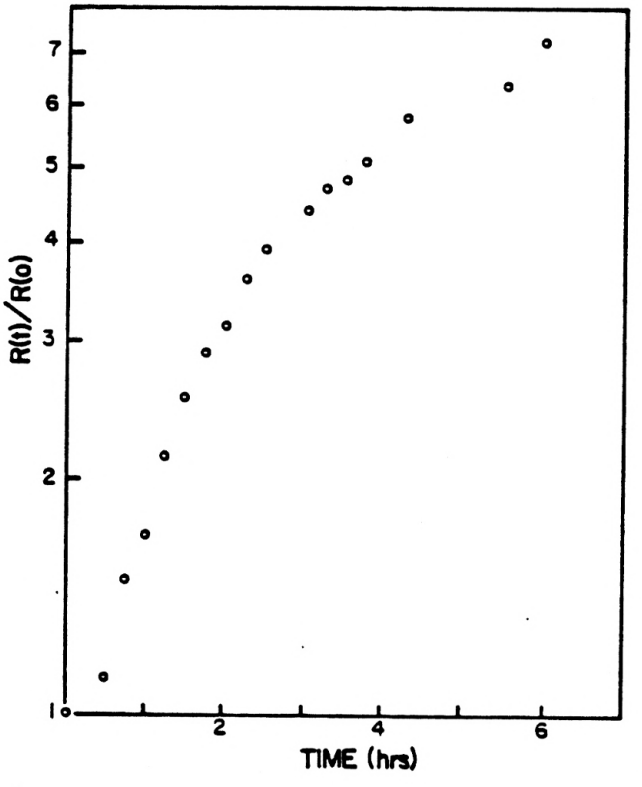

Fig. 4.2b
Average rate of growth vs. aggregation time for sol number 2.

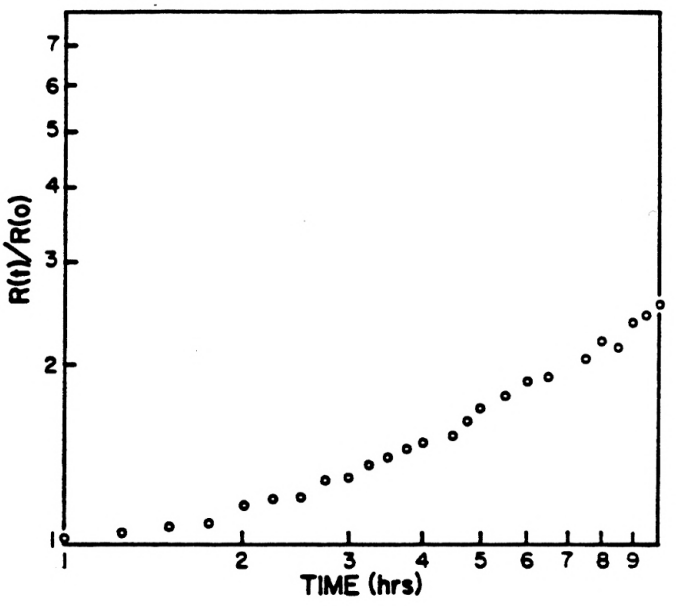

Fig. 4.1c
Average rate of growth vs. aggregation time for sol number 3. $T_a \approx 4$ hrs and $(z/d_f)_{T_a} \approx .5$

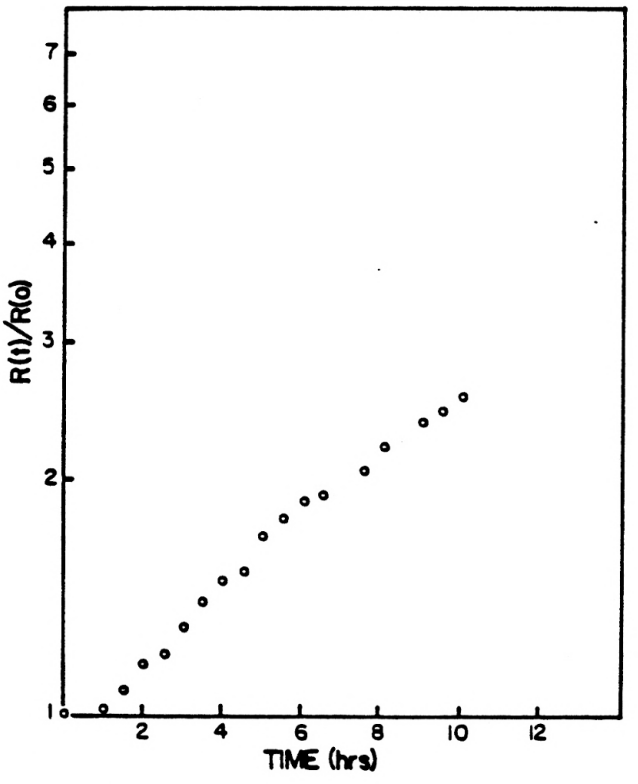

Fig. 4.2c
Average rate of growth vs. aggregation time for sol number 3.

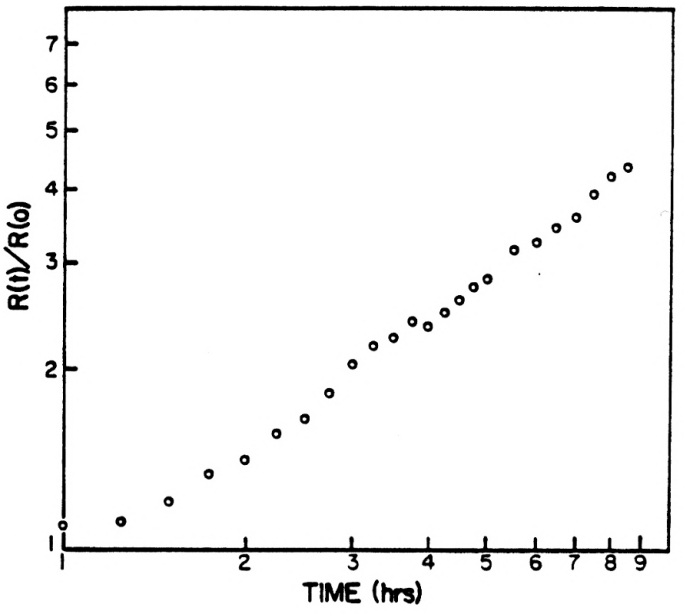

Fig. 4.1d
Average rate of growth vs. aggregation time for sol number 4. $T_\infty \approx 2.5$ hrs and $(z/d_f)_{T_\infty} \approx .7$

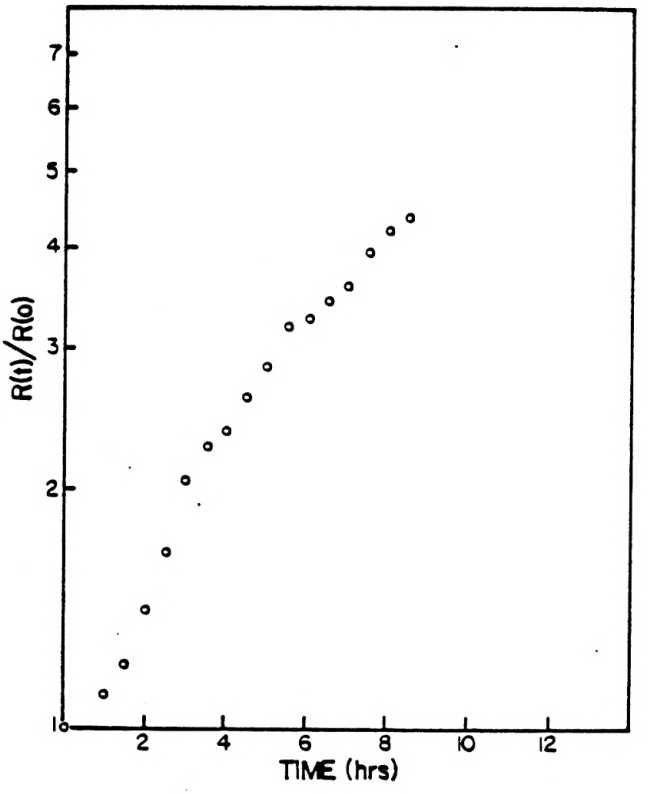

Fig. 4.2d
Average rate of growth vs. aggregation time for sol number 4.

Fig. 4.1e
Average rate of growth vs. aggregation time for sol number 5. $T_a \simeq 2$ hrs and $(z/d_f)_{T_a} \simeq 1.0$

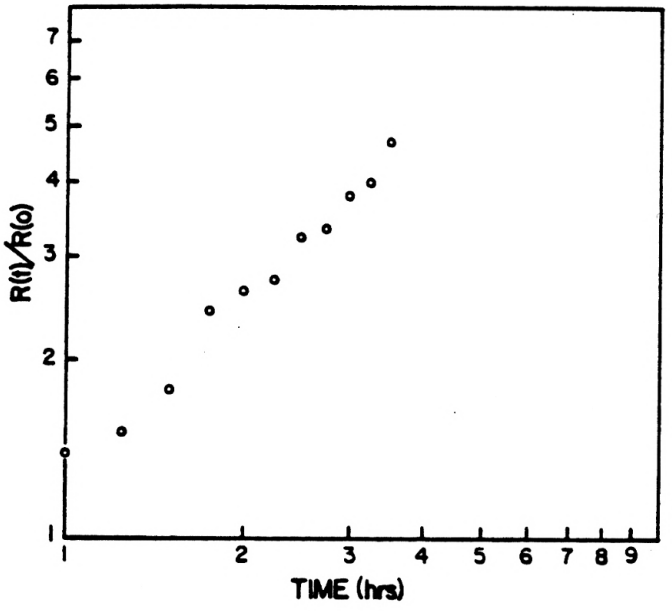

Fig. 4.2e
Average rate of growth vs. aggregation time for sol number 5.

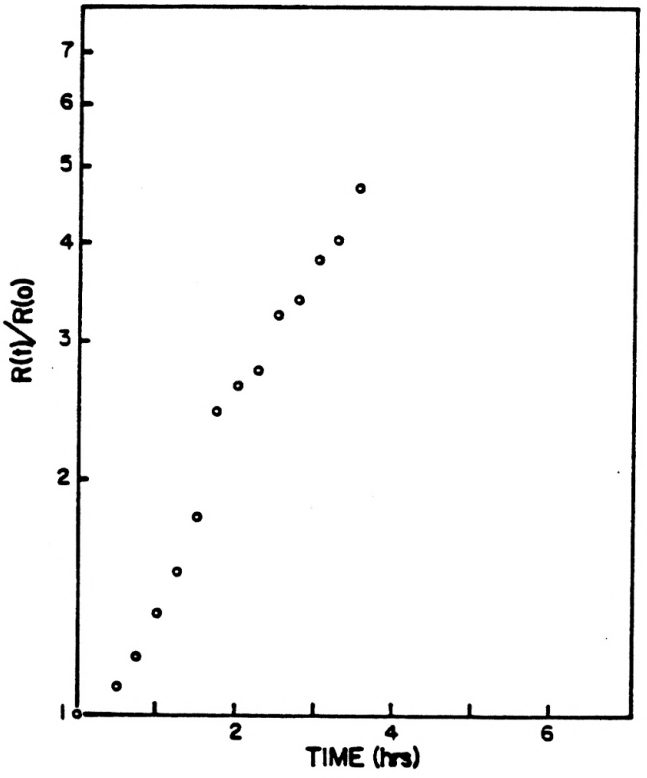

plots [see Figs. 4.1a, 4.1b, 4.1c, 4.1d and 4.1e]. These results confirm recent findings from Weitz et al.[16,17]

The general expression for the dynamic exponent z was

$$z = 1/(1-\lambda) \ . \qquad (2.41)$$

It is well known that the fractal dimension for a gold aggregate is bounded by $1.75 \leq d_f \leq 2.05$.[16,17] Using Eq. (2.41) and an average fractal dimension of 1.9 we take the known values for z/d_f and calculate the kernel homogeneities for the five sols. These results are summarized in Table 4.2.

Table 4.2

Sol No.	λ
1	$.12\pm.07$
2	$.24\pm.05$
3	$.09\pm.08$
4	$.29\pm.06$
5	$.47\pm.04$

Figures 4.4a, 4.4b, 4.4c, 4.4d, and 4.4e are linear plots of the polydispersity index Q against aggregation time. All the plots seem to indicate that Q has approached an asymptotic value independent of time. These findings are summarized in Table 4.3.

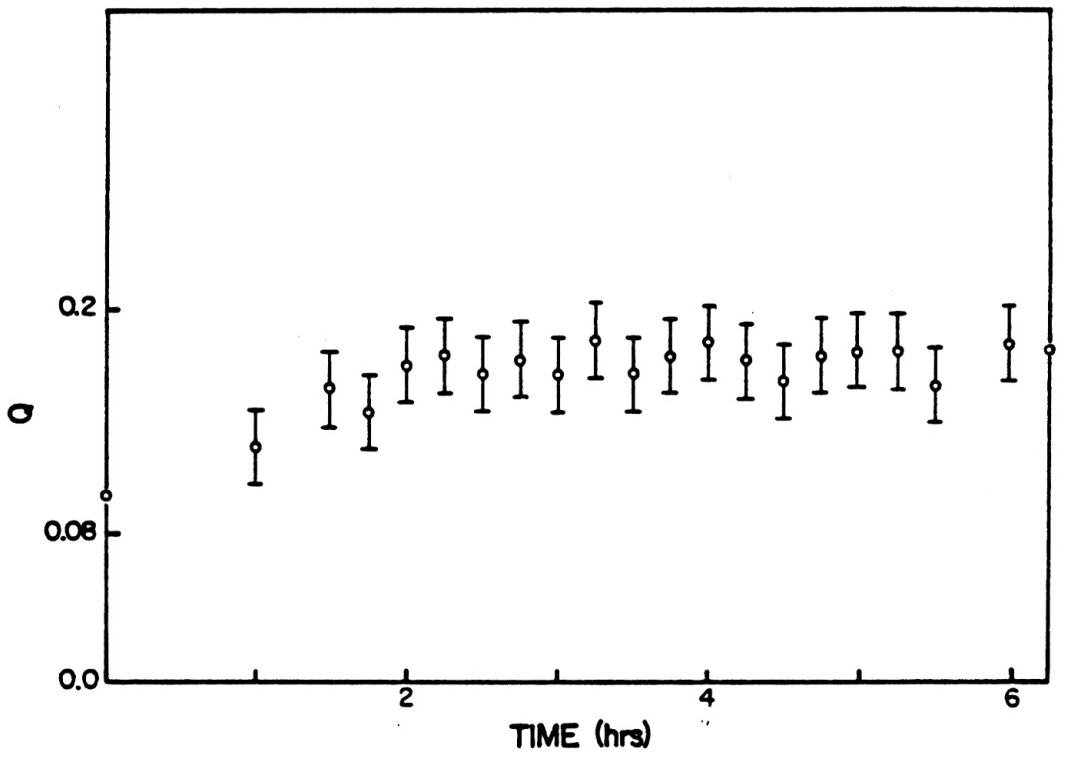

Fig. 4.4a Polydispersity index Q vs. aggregation time for sol number 1, $Q_\infty \simeq .17$

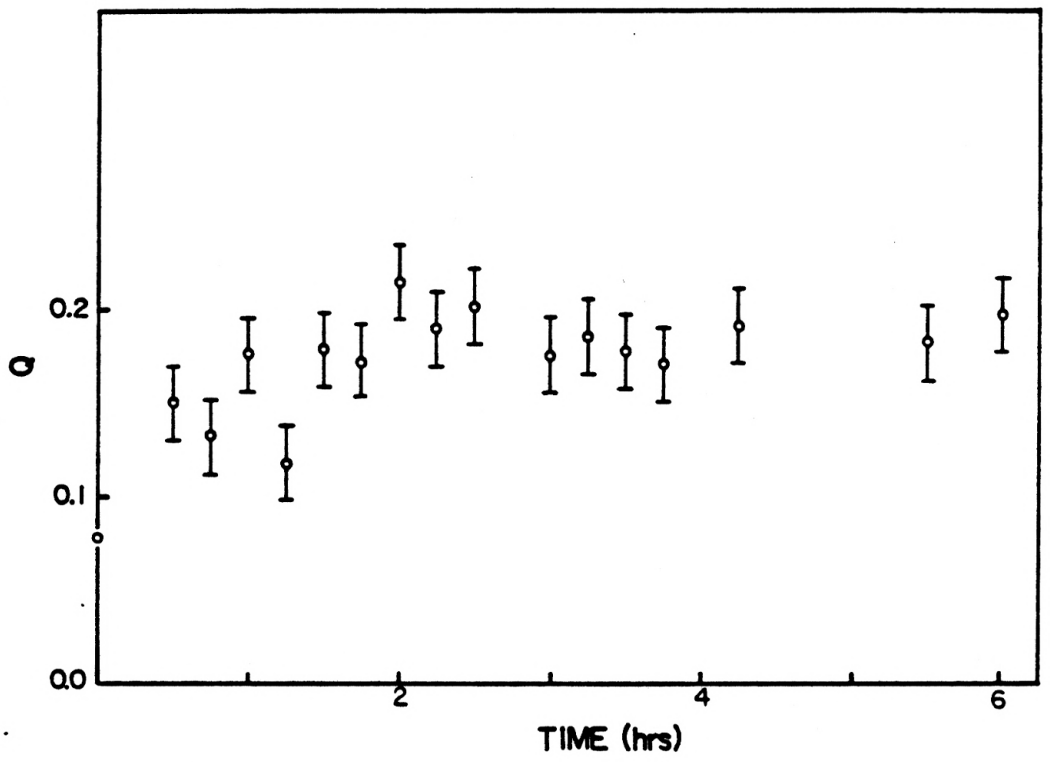

Fig. 4.4b Polydispersity index Q vs. aggregation time for sol number 2, $Q_\infty \simeq .19$.

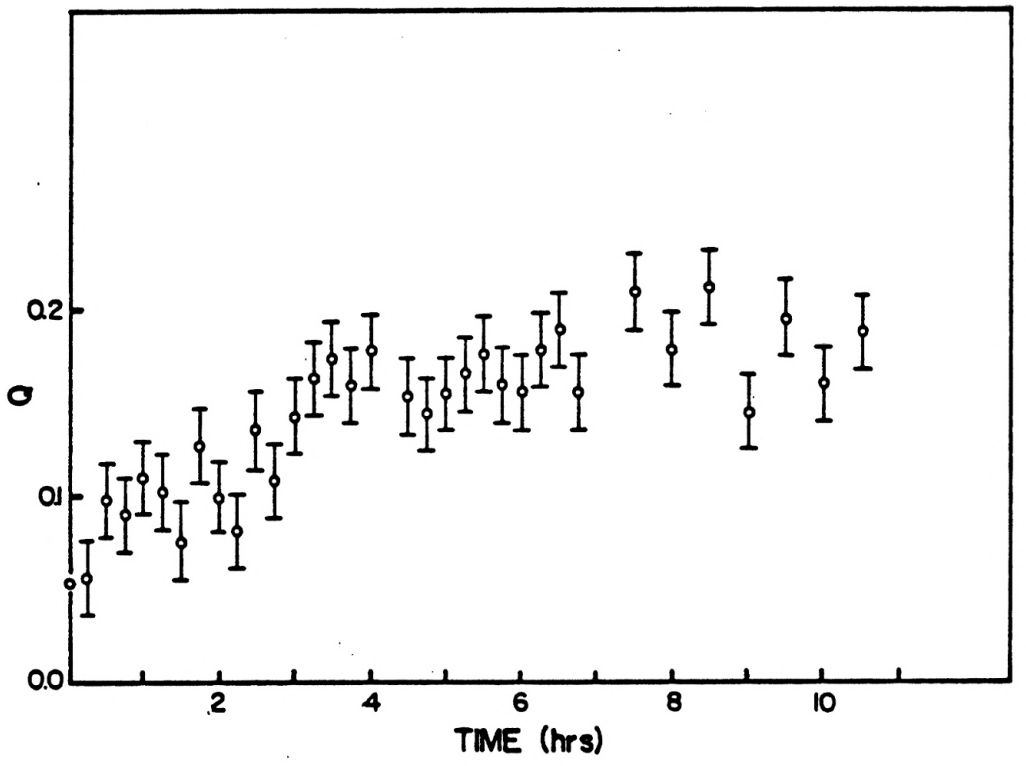

Fig. 4.4c Polydispersity index Q vs. aggregation time for sol number 3, $Q_\infty \simeq .18$

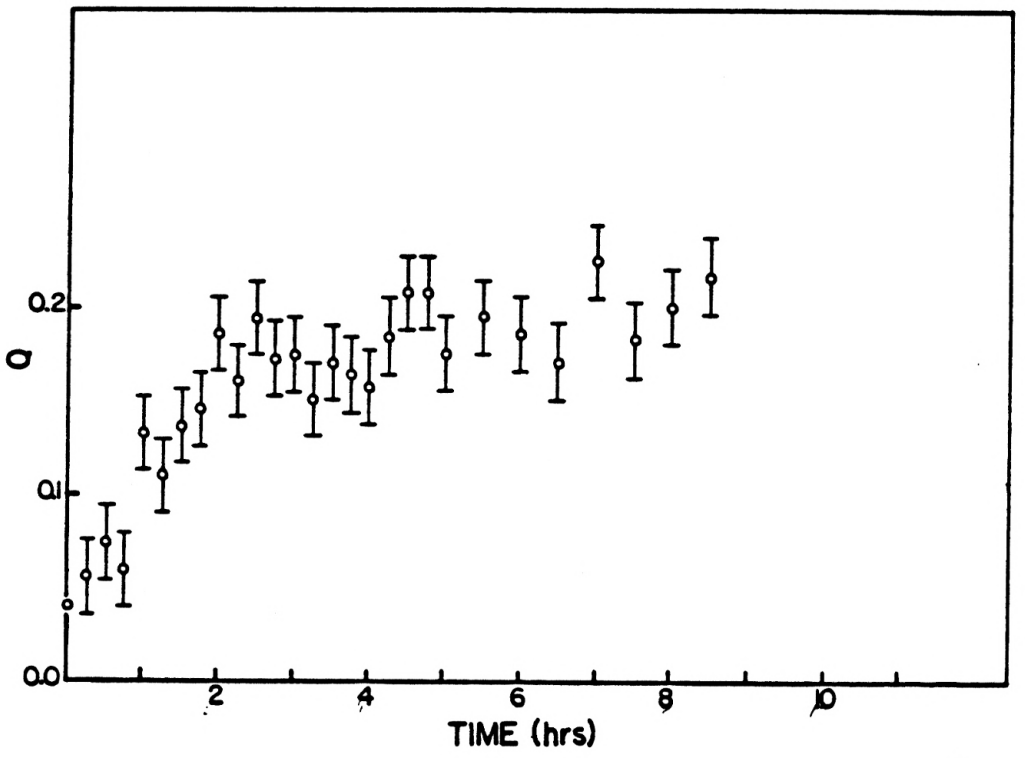

Fig. 4.4d Polydispersity index Q vs. aggregation time for sol number 4. $Q_\infty \simeq .19$

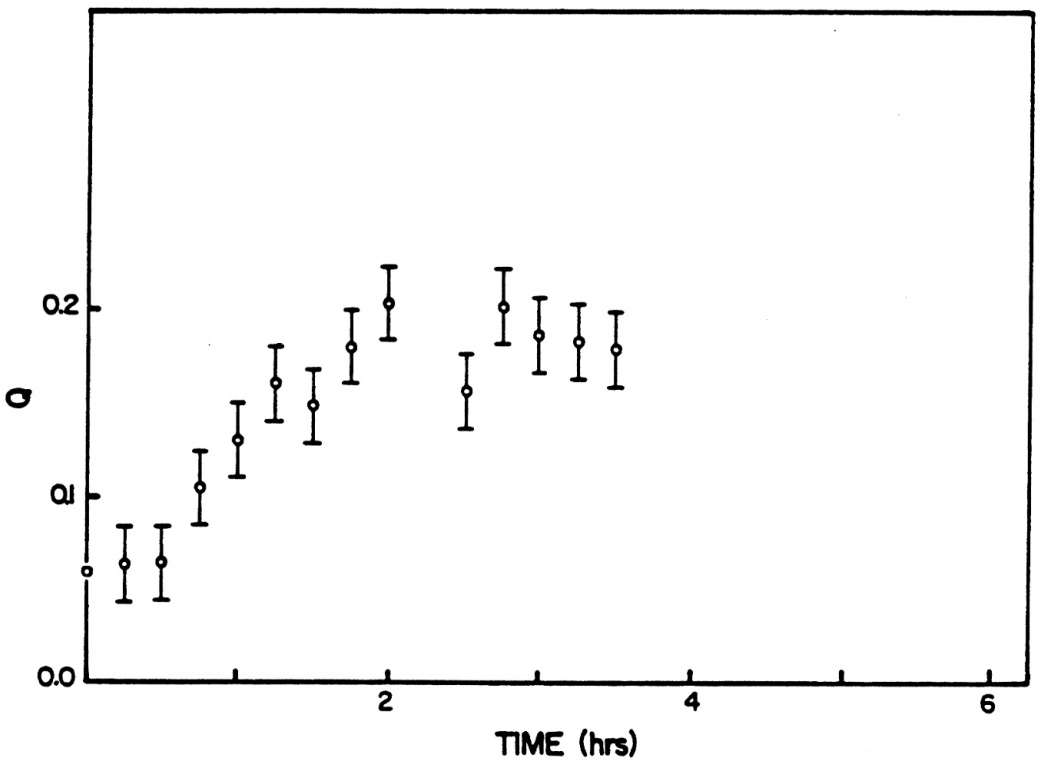

Fig. 4.4e Polydispersity index Q vs. aggregation time for sol number 5, $Q_\infty \simeq .19$

Table 4.3

Sol No.	Q_∞(Exp)	Q_∞(Theory)	λ
1	.17	.16	.1
2	.19	.17	.2
3	.17	.16	.1
4	.19	.19	.3
5	.19	.21	.5

In Table 4.3, Q_∞(Exp) represents experimentally determined asymptotic values for Q, and Q_∞(Theory) represents the calculated asymptotic values for Q as predicted by the B-J distribution [see Eq. (2.73) and Fig. 2.3]. Again, an average fractal dimension of 1.9 was used. Table 4.3 indicates good agreement between the asymptotic Q values from experiment and those calculated from the B-J distribution.

CHAPTER 5

Conclusion

The time evolution of the intensity-weighted relative normalized moment of Q is an effective measure of the evolution of a cluster size distribution's shape. A constant value for the moment Q implies a constant shape for the cluster distribution. Physically, the constant shape means a scaling distribution. During aggregation, Q was found to evolve from an arbitrary initial value into a final constant one. This behavior for Q was present in all five aggregated colloidal gold suspensions implying that all five cluster distributions had scaled. Within experimental error, the same asymptotic Q values resulted.

The validity of the experimentally found constant values for Q become apparent when compared with those calculated from the asymptotic B-J distribution. The constant, scaling values for Q predicted by the B-J distribution were within 10% of those found experimentally for an average fractal dimension of 1.9 and kernel homogeneities ranging from 0.1 to 0.5. From the excellent agreement between experiment and theory, we conclude that the B-J distribution accurately represents the large mass ends of the scaling distributions in our gold sols.

The intensity-weighted moment μ_1 was found to obey a dynamic power law scaling relation characterized by the exponent z and fractal dimension d_f, i.e. $\mu_1 \sim t^{-z/d_f}$. The power law scaling of μ_1

occurred at the approximate aggregation time that Q went asymptotic for all five gold sols. Hence, the static scalings of the five distributions as indicated by the unchanging values for Q implied dynamic scaling of the moments as well. This power law behavior for μ_1 is predicted by the Vicsek and Family scaling Ansatz.

Dynamic light-scattering is an effective probe for measuring the time evolution of intensity-weighted moments from cluster size distributions. Hence, this technique has proven useful for monitoring the time evolution of a cluster size distribution into its scaling form.

References

[1]T.A. Witten, Jr., L.M. Sander, Phys. Rev. Lett. 47, 1400 (1981).

[2]B. Mandelbrot, The Fractal Geometry of Nature (W.H. Freeman, San Francisco, 1982).

[3]T. Vicsek, F. Family, Phys. Rev. Lett. 52, 1669 (1984).

[4]G.K. vn Schulthess, G.B. Benedek, R.W. DeBlois, Macromolecules 13, 939 (1980).

[5]D.A. Weitz, M.Y. Lin, Phys. Rev. Lett 57, 2037 (1986).

[6]T. Vicsek, F. Family, Kinetics of Aggregation and Gelation (North-Holland, Amsterdam, 1984).

[7]P.G.J. van Dongen, M.H. Ernst, J. Colloid Interface Sci. 115, 27 (1987).

[8]K. Kang, S. Redner, P. Meakin, F. Leyvraz, Phys. Rev. A. 33, 1171 (1986).

[9]P.G.J. van Dongen, M.H. Ernst, Phys. Rev. Lett. 54, 1396 (1985).

[10]R. Botet, R. Jullien, J. Phys. A: Math Gen. 17, 2517 (1984).

[11]C.M. Sorensen (private communication).

[12]B.J. Berne, R. Pecora, Dynamic Light-Scattering, (John Wiley & Sons Inc., New York, 1976).

[13]D.E. Koppel, J. Chem. Phys. 57, 4814 (1972).

[14]P. Wiltzius, Phys. Rev. Lett. 58, 710 (1987).

[15]C.M. Sorensen, T.W. Taylor, Phys. Rev. A 33, 1411 (1986).

[16]D.A. Weitz, T.S. Huang, M.Y. Lin, J. Sung, Phys. Rev. Lett 53, 1675 (1984).

[17]D.A. Weitz, J.S. Huang, M.Y. Lin, J. Sung, Phys. Rev. Lett 54, 1416 (1985).

[18]B.V. Enustun, J. Turkevich, T. Am. Chem. Soc. 85, 3317 (1963).

[19]J. F. Merklin (private communication).

[20]T.W. Taylor, S.M. Schrivner, C.M. Sorensen, J.F. Merklin, Applied Optics 24, (1985).

IN SITU MEASUREMENTS OF THE APPROACH TO SCALING OF COLLOIDAL CLUSTER SIZE DISTRIBUTIONS DURING AGGREGATION

By

Bernard J. Olivier

B.S., Bates College, 1983

AN ABSTRACT OF A MASTER'S THESIS

submitted in partial fulfillment of the

requirements for the degree

MASTER OF SCIENCE

Department of Physics

KANSAS STATE UNIVERSITY
Manhattan, Kansas

1987

ABSTRACT

Cluster size distributions in aggregating colloidal suspensions are believed to evolve out of arbitrary initial shapes into a final self-preserving or scaling form. This final scaling form is dependent upon the collision kernel responsible for the aggregation.

The scaling of a cluster distribution is characterized by its relative normalized moments. The relative normalized moments of a scaling distribution are independent of time. In this thesis dynamic light-scattering, which is a probe of these relative normalized moments, was used to measure the time evolution of cluster distributions in aggregating gold colloids.

Quasi-monodisperse gold sols were prepared and then aggregated. During the aggregation, photon correlation spectroscopy was used to measure the time evolution of the intensity-weighted moments μ_1 and μ_2 of the cluster size distributions. The dynamic behavior of μ_1 and μ_2 was used to identify the cluster distribution's approach to a scaling form. In particular, the effective width for a cluster distribution can be parameterized with a ratio of these moments $Q \equiv \mu_2/\mu_1^2$. The index Q is an intensity-weighted relative normalized moment. Q was found to evolve from arbitrary initial values to nearly the same final value for each of the sols. This indicated the cluster size distributions in these sols had taken on scaling shapes.

The experimental asymptotic values for Q agreed well with theoretical predictions, using a scaling distribution derived by Botet and Jullien, for a cluster fractal dimension of 1.9 and range of kernel homogeneities from .1 to .5.